Investigation of Volatiles in Rhyolitic Magma Chambers

by
Nelia W. Dunbar

An Independent Study submitted to the Faculty of
New Mexico Institute of Mining and Technology
in partial fulfillment of the requirements for the
Master of Science Degree

Department of Geoscience
New Mexico Institute of Mining and Technology
August, 1985.

Table of Contents

List of Figures

List of Tables

ABSTRACT

Tephra from the Taupo and Okataina Volcanic Centers of the Taupo Volcanic Zone, New Zealand contain obsidian, crystals and pumice. H_2O and Cl were measured in obsidian, and Cl was determined from glass inclusions within phenocrysts, in order to examine the pre-eruptive volatile contents of rhyolitic magma.

H_2O in rhyolitic obsidian varies from 0.3 to 2.6 wt.%. A degassed obsidian sample from a local rhyolitic flow contains 0.1 wt.% H_2O, close to estimates for atmospheric equilibrium of water in silicate glass determined by Taylor et. al. (1983). A single delta D value of -70 permil on water from an obsidian sample is typical of magmatic water and is unlike the local meteoric water. The high water contents and delta D value suggest that the obsidian clasts are cogenetic with the non-lithic portion of the tephra. This obsidian is thought to quench under special conditions which limit degassing, so the volatiles in this glass represent a part of the pre-eruptive volatile content of the magma.

The glass inclusions in phenocrysts are chemically similar to the obsidian but are enriched in Cl. The Cl in melt inclusions ranges from 0.18 to 0.24 wt.%, averaging 0.19 wt.%, whereas in the obsidian clasts the range is from 0.12 to 0.17 wt.%, averaging 0.14 wt.%. There is a positive correlation between the average water and Cl contents in obsidian fragments

from the same eruption, suggesting that the two volatile species degas at approximately the same rate. By extrapolating this correlation, and using the Cl content of the glass inclusions, an original magmatic water content of between 2.5 and 4.0 wt.% has been estimated.

Temperature and oxygen fugacity calculated from co-existing magnetite and ilmenite compositions were determined for most of the tephra units, giving ranges of 750 to 930°C and log fO_2 of -11 to -15. Temperature plotted against oxygen fugacity show trends which parallel the QFM trend, but are 1 to 2 log units higher. The Taupo and Okataina centers cover roughly the same span of values, but fall on two distinct buffer trends, indicating derivation from separate magma types. The highly explosive Taupo plinian unit gives higher temperatures than deposits from associated plinian eruptions. Heating stage geothermometry studies on two phase melt inclusions yield melt temperatures close to those from Fe-Ti oxides. Decrepitation of inclusions occurs soon after melting, probably indicating that the trapping pressure was high.

INTRODUCTION

Volatile elements in magmas are important to a number of magmatic processes. As volatile components exsolve from a melt at low pressure, and expand, they act as a driving force for energetic volcanic eruptions, such as fire fountaining from basaltic magmas and large scale plinian and ignimbrite eruptions from silicic melts (Fisher and Schmincke, 1984). The petrogenetic evolution of magmas is affected by the quantity and composition of volatiles, because dissolution of these elements controls the degree of polymerization of the melt, thereby influencing the crystallization patterns (Burnham, 1979). Magmatic volatiles are important in the formation of hydrothermal ore deposits because they can complex with ore metals which are then transported in solution (Barnes, 1979). Finally, certain magmatic volatiles which are emitted during volcanic eruptions can have a severe environmental impact, and should be considered among volcanic hazards (Rampino and Self, 1984).

Although volatiles are important, they are difficult to assess quantitatively within magma chambers. However, there are a number of ways to experimentally estimate pre-eruptive volatiles. These methods include: analyses of gasses emitted from active volcanoes (Gerlach, 1981); volatile determinations in volcanic products which could trap magmatic volatiles, such as obsidian (Eichelberger and Westrich, 1981), deep sea basalts (Moore, 1970), or glass inclusions in magmatic phenocrysts

(Sommer and Schramm, 1983); experimental estimates based on petrologic characteristics (Merzbacher and Eggler, 1984); and thermodynamic calculations from mineral equilibria reactions (Ewart et. al., 1975). Details of these methods along with more information about volatiles are discussed in Appendix A.

The objective of this study was to determine the H_2O and Cl contents of rhyolitic magmas. The degassing behavior and absolute quantities of these volatiles was investigated by analysing quenched volcanic glass (obsidian), which has been shown in other cases to have not completely degassed and to contain some percent of pre-eruptive volatiles (Eichelberger and Westrich, 1981). Glass inclusions trapped in magmatic phenocrysts were analysed as these should reflect the pre-eruptive content of volatiles in the magma (Roedder, 1984).

Obsidian may undergo different degrees of degassing during eruption (Eibbchelberger and Westrich, 1981). Completely degassed obsidian, such as would be found in an obsidian dome or flow, contains about 0.2 wt. % H_2O (Taylor et. al., 1983). Eichelberger and Westrich (1981) studied obsidian from several rhyolitic volcanic sequences in California, and, based on water contents of 0.5 to 1.0 wt. %, postulated that this material cooled and quenched under special conditions which limited degassing. Degassed flow material from the same eruptive sequence contains 0.1 to 0.2 wt. % H_2O (Eichelberger and Westrich, 1981). Taylor et. al. (1983) reinforce this

conclusion, by showing that delta D values from water contained in obsidian follow a Raleigh fractionation trend with increased degrees of degassing, showing typical magmatic values of -70 permil at 3.0 wt.% H_2O, but ranging as low as -130 permil at 0.2 wt.% H_2O due to degassing. This trend suggests that obsidian fragments undergo various degrees of degassing before quenching during the eruption, and indicates that some obsidians may contain close to the original premagmatic volatile content.

Melt (or glass) inclusions trapped during growth of phenocrysts may contain representative pre-magmatic volatiles if no exsolution bubble grows prior to quenching (Sommer, 1979). Volatiles in glass inclusions have been sucessfully analysed by a number of workers, in particular H_2O by Sommer and Schramm (1984), as well as S and Cl by Devine et. al. (1984).

The Taupo Volcanic Zone, in the central North Island of New Zealand (Fig. 1), was chosen for this study because of the large number of large explosive volcanic eruptions from several different centers which have occurred in the last 40,000 years (Froggatt, 1982). The stratigraphy, petrology and chemistry of these deposits have been studied (Ewart, 1963, 1966; Ewart et. al., 1971, 1975; Froggatt, 1981; Howorth, 1976; Nairn, 1972, 1980, 1981; Vucetich and Howorth, 1976; Vucetich and Pullar, 1969, 1973; Wilson et. al., 1980, 1984). The eruptive nature of these volcanoes has been well studied, and one eruption has been classified as "ultraplinian", based on a dispersal versus

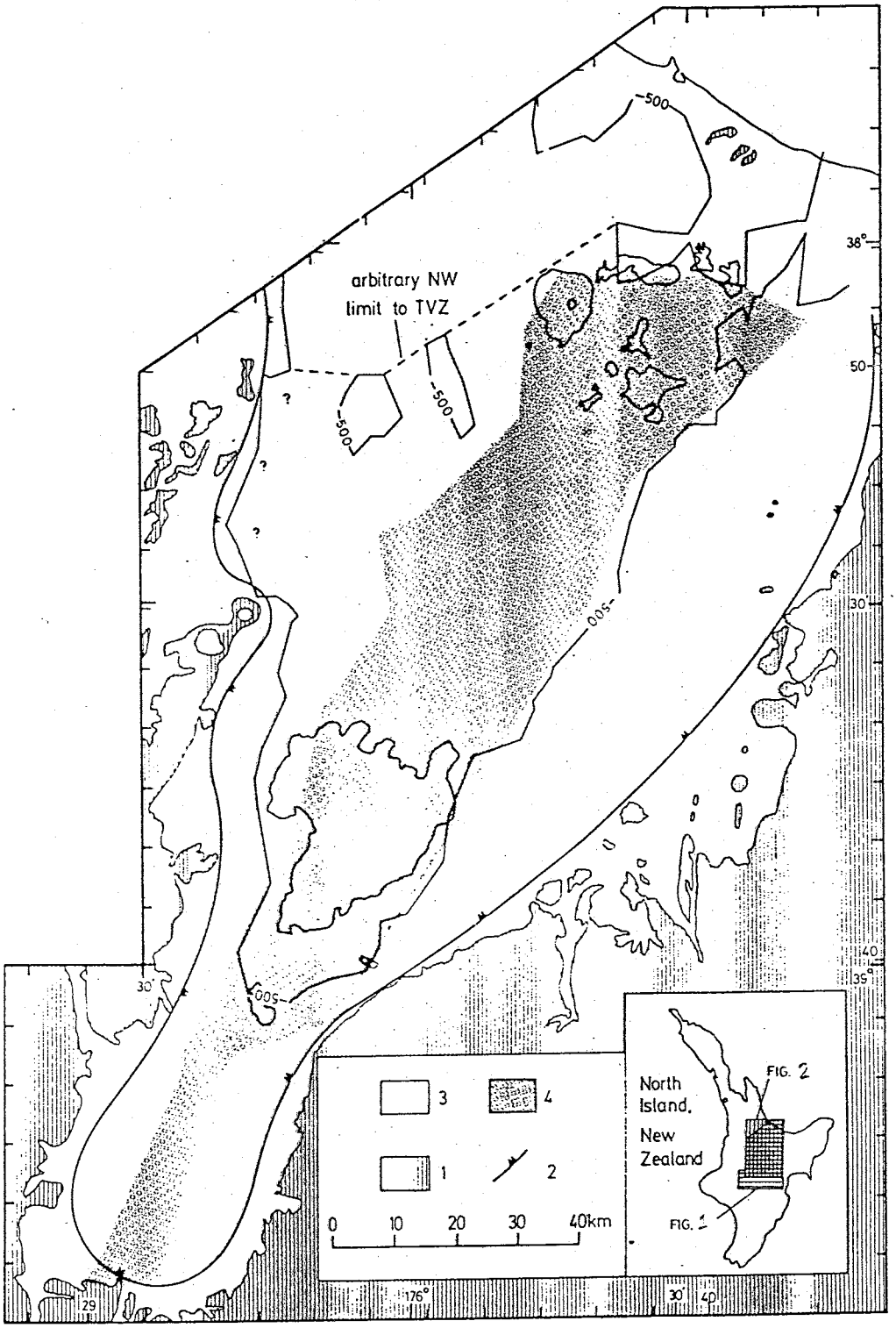

Figure 1. Map of onshore areas affected by volcanism and basement collapse of the Taupo Volcanic Zone.

Key:
1) basement greywacke and Tertiary marine sediments
2) outer margin of basement collapse
3) area of inferred vents
4) areas of vents active during the past 150 ky.

500 m. below sea level contour is shown

From Wilson et. al, 1984

fragmentation index (Walker, 1980, 1981). The amount of material ejected per eruption has been calculated for most units, as has the aerial distribution of deposits (Froggatt, 1982; Nairn, 1980, 1981; Vucetich and Howorth, 1976; Vucetich and Pullar, 1973; Walker, 1980, 1981; Wilson, 1984). Ignimbrites are associated with some airfall deposits. Eichelberger and Westrich (1981), and Taylor et. al. (1983) studied the degassing behavior of obsidian for small volume eruptions. This study will determine if the same processes occur in large scale events. The TVZ plinian deposits are ideal for a study of the quantity and behavior of volatiles in magma.

TAUPO VOLCANIC ZONE

Introduction

The Taupo Volcanic Zone (TVZ), in the central North Island of New Zealand covers 200 by 40 km., and contains at least 6 major calderas (Fig. 2) (Wilson et. al., 1984). It is an area of back-arc-subduction-related extension and subsidence, with rates of 0.7 and 0.3 cm./yr., respectively (Cole, 1984). The tensional regime in the North Island, particularly in the Taupo-Rotorua depression, is a result of oblique subduction of the Pacific plate under the Indian plate (Cole, 1984). This tension results in an extensional ensialic basin which has produced over 10,000 $km.^3$ of rhyolitic volcanic material as well as associated andesites and basalts over the last million years (Cole, 1984). The crust in the TVZ is approximately 15 km. thick compared to 30-35 km. outside the basin, and consequently, heat flow is high (Cole, 1984; Stern, 1985). A large part of the volcanism has been concentrated in 6 calderas shown in Fig. 2; Rotorua, Okataina, Kapenga, Mangakino, and Taupo. These calderas are not obvious structures, but have been defined by depressed areas in the underlying basement rocks, and clustering of eruptive vents (Wilson, 1984). No evidence of resurgent doming is seen in the TVZ (Wilson, 1984).

Two major theories have been proposed for the genesis of the large volumes of rhyolite present in the TVZ (Cole, 1979). The first, fractional crystallization of TVZ andesites or high-Al

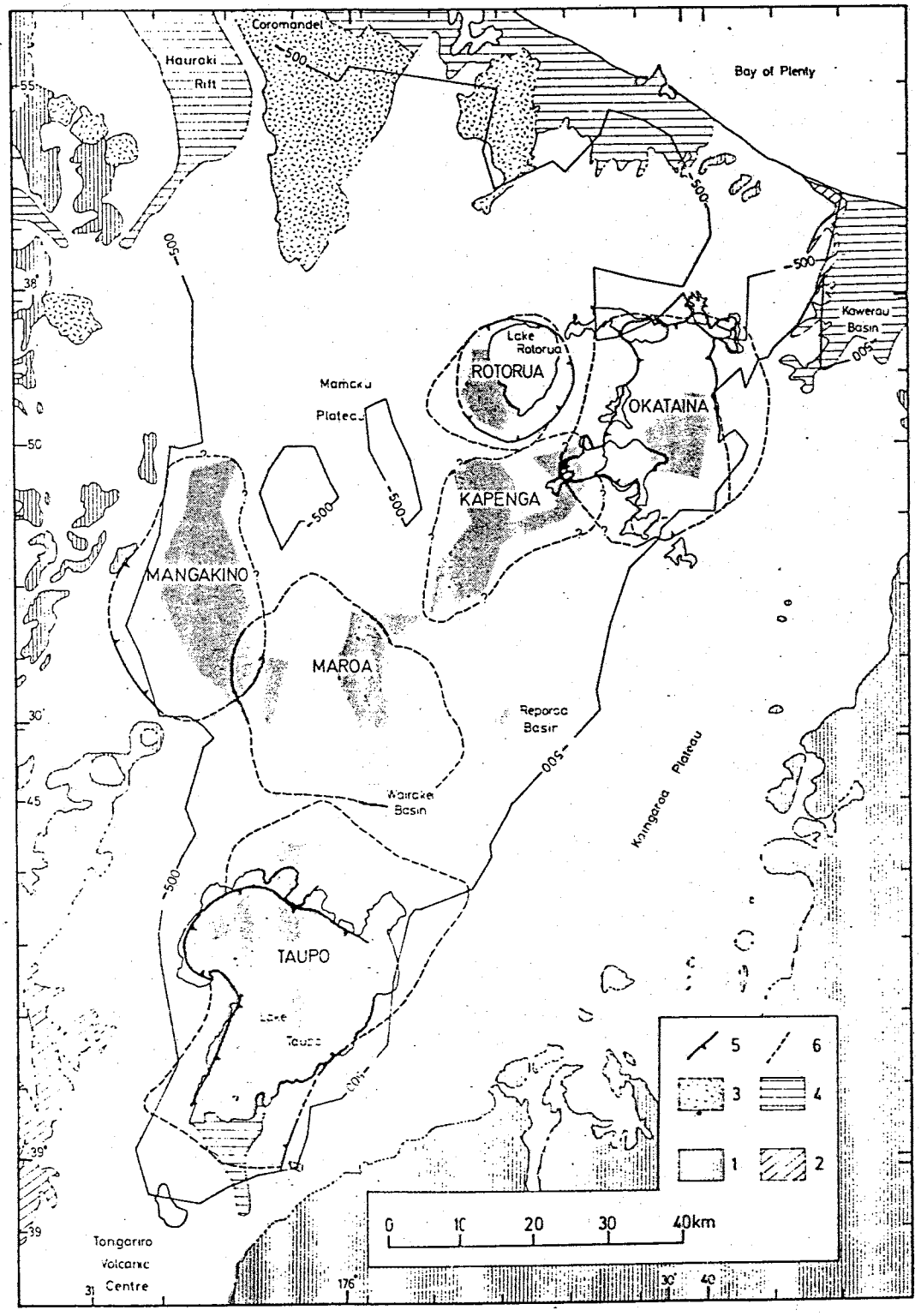

Figure 2. Location map of rhyolitic calderas and associated tectonic basins in the TVZ.
Key:
1) basement greywacke 2) Tertiary to Quaternary marine sediments
3) Pliocene-Pleistocene volcaincs predating or synchronous with early TVZ activity 4) young sediments 5) caldera margins 6) outer limits of named calderas.
500 m. below sea level contour is shown

From Wilson et. al., 1984

basalts, is geochemically feasible, but does not seem possible when the large volume is considered. Eighty-eight percent fractional crystallization of a basaltic lava is necessary to generate the correct rhyolitic chemistry, and this would leave a huge volume of residue, for which there is no evidence (Cole, 1979). Isotopic evidence is also against this origin (Blattner and Reid, 1982). The second possibility, partial melting of basement rocks, seems more probable. Taupo rhyolites can be generated by 35% partial melting of a metamorphic greywacke, based on major, trace element, and isotopic analyses (Cole, 1979).

Occurrence

The tephra studied in this project are from the Taupo Volcanic Center (TVC) and the Okataina Volcanic Center (OVC). Most tephra from these centers which are less than 40,000 yrs. old have been sampled, but those which are less than 20,000 yrs. old are the best units for this study because the young age reduces the probability that the obsidians are hydrated.

Volumes of Tephra

The volume of tephra from each eruption has been determined by a number of workers, sometimes with conflicting results (Tables 1 and 2). Age, source, crystal content and other details for each tephra unit are also given in Tables 1 and 2. Vucetich

Table 1. Major tephra units in the Taupo Volcanic Center

Name of Unit	Age ky B.P.	Volume (km^3) a	b	c	d	Mineralogy plag.	pyx.	amph.	biot.	Assoc. Ignimbrite	References
Taupo plinian	2	12.2	12+	-	24	H	H	VL	-	yes	a,b,d,e
Rotongaio	2	3.3	1	-	-	H	H	VL	-	-	a,b,e
Hatepe phreato.	2	3.2	-	-	-	H	H	VL	-	-	a,e
Hatepe plinian	2	4.7	2	-	6	H	H	VL	-	-	a,b,d,e
Marapa	2.2	-	2	0.65	-	H	H	VL	-	-	b,c,e
Whakaipo	2.8	-	1.5	0.8	-	H	H	VL	-	-	b,c,e
Waihimia	3.2	-	14	15	29	H	H	VL	-	yes	b,c,d,e
Hinimaiaiai	4.7	-	3	4.7	-	H	H	VL	-	-	b,c,e
Motutere	5.4	-	0.5	-	-	H	H	VL	-	-	b,e
Opepe	8.8	-	4	5	-	H	H	VL	-	yes	b,c,e
Porunui	9.5	-	3	3.5	-	H	H	VL	-	-	b,c,e
Karapiti	9.8	-	2	5	-	H	H	VL	-	yes	b,c,e
Oruanui*	20	-	70	-	-	H	H	M	VL	yes	b,e
Okaia	22	-	-	-	-	H	H	M	VL	-	e
Tihoi	38	-	-	-	-	H	H	M	VL	-	e

* Self and Sparks (1978) report a volume of 75 km^3 for the plinian tephra associated with the Oruanui ignimbrite

Mineral Abundances
H = high
M = moderate
L = low
VL = very low

Mineral Types
plag. = plagioclase
pyx. = pyroxene
amph. = amphibole
biot. = biotite

References: a) Froggatt, 1981; b) Froggatt, 1982; c) Vucetich and Pullar, 1973; d) Walker, 1981; e) Froggatt, 1983

Table 2. Major silicic tephra units sampled from the Okataina Volcanic Center

Name of Unit	Age ky B.P.	Volume (km^3) a	Volume (km^3) b	Mineralogy plag.	Mineralogy pyx.	Mineralogy amph.	Mineralogy biot.	Assoc. Ignimbrite	References
Kaharoa	0.93-0.65	4	5	H	L	L	M	-	a,b,d
Whakatani	5.5	6	10	H	M	M	-	-	a,b,d
Mamaku	7.5	6	-	H	M	M	L	yes	a,d
Rotoma	9	12	12	H	M	M	L	-	a,b,e
Waiohau	11	-	13.8	H	M	M	L	yes	b,d
Rotarua	13	7	6.7	H	M	M	L	yes	a,b,d
Rerewnakaaitu	14.7	7	5.8	H	M	M	M	yes	a,b,e
Okareka	17	8	8	H	L	M	M	-	a,b,d
Terere	19	9	-	H	M	M	-	-	a,d
Omateroa	28	16	18	H	M	M	-	yes	a,b,c
Awakeri	30	2	2	H	L	H	-	-	a,b,c
Mangaone	31	16	-	H	M	M	-	yes	a,c

Mineral Abundances
H = high
M = medium
L = low

Mineral Types
plag. = plagioclase
pyx. = pyroxene
amph. = amphibole
biot. = biotite

References: a) Froggatt, 1982, b) Nairn, 1981, c) Howorth, 1976, d) Nairn, 1980, e) Topping and Kohn, 1973.

and Pullar (1973), calculated a number of volumes for the TVC tephra, applying the formula $13ab^2$, where "a" is the thickness of tephra at source, and "b" is the distance over which tephra thickness is halved. Nairn (1981) has determined volumes for the OVC, presumably by the same method. Froggatt (1982) has done a study, comparing 4 different volume determination methods, yielding average volume values for both the TVC and OVC. Walker (1981) reports values for several tephra units from the TVC, using the crystal concentration method, which is based on the assumption that the crystals versus glass in a pumice clast is representative of that for the entire magma, and from the measured crystal content of a tephra unit, the total glass volume can be calculated. This method yields much higher values than all others, but Walker explains that a high percentage of material is lost as fine dust and never is considered in normal volume calculations.

The eruption rates for the TVC and OVC over the last 32,000 years are quite different (Fig. 3). TVC eruptions are either large or small in volume, and are clustered through time, whereas most OVC eruptions were of moderate volume, and occur at relatively constant time intervals. The OVC maintained a steady state of magma eruption whereas the TVC followed a step function (Froggatt, 1982). The combined volume of rhyolitic material erupted from these two centers over the last 50 ky is 350 $km.^3$ (Froggatt, 1982).

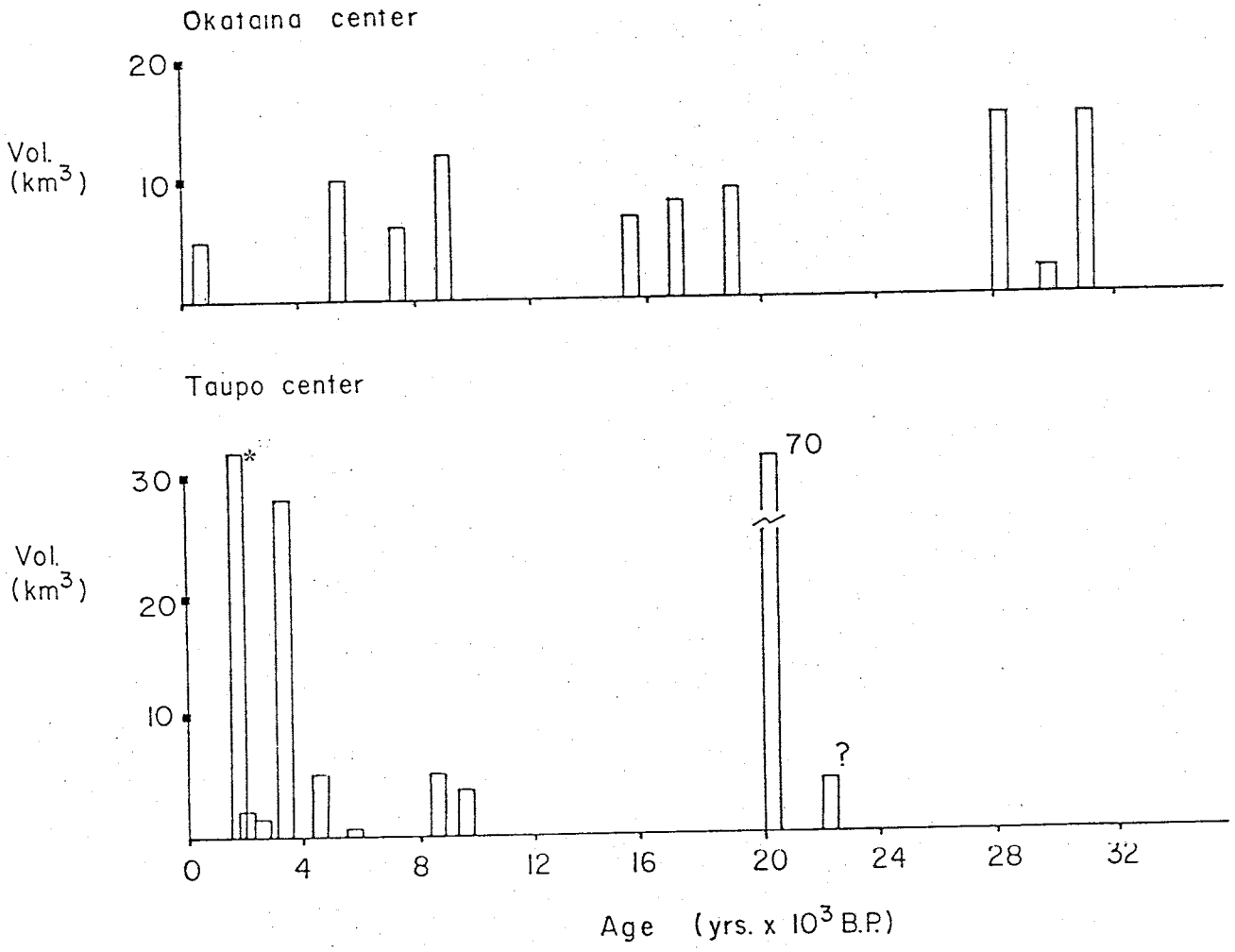

Figure 3. Volumes of rhyolitic tephra erupted from the Taupo and Okataina volcanic centers.

* This volume represents combined eruptive material from the 4 eruptions which occurred about 2000 yrs. B.P.: Taupo plinian, Rotongaio, Hatepe phreatomagmatic, and Hatepe plinian.

Mineralogy

Tephra from the TVC and OVC are composed of pumice, glass fragments, plagioclase, mafic silicates (pyroxene and amphibole), magnetite, ilmenite and occasional biotite (Froggatt, 1983). Although there are slight differences through time, the chemical composition of TVZ eruptive products are very constant. There is no evidence of significant chemical zonation in the magma chamber within, or between eruptions (Ewart, 1963; Froggatt, 1983).

Previous studies by Ewart (1963), and Ewart et. al. (1971, 1975), have suggested that TVZ rhyolitic magmas began crystallization under saturated conditions, where $P_{H2O} = P_{total}$. These studies were based on equilibria of mineral phases present in the extruded rhyolite. They determined that the vapor pressure in the magma chamber was 2000 to 3000 kg./cm.^{2}, confining pressure of the magma chamber was 2.5 kb., so crystallization occurred at depths of between 5 and 7 km.

Volatile Determinations

Ewart et. al. (1975), and Rutherford and Heming (1978), have suggested H_2O contents of between 5 and 8 wt.% for some TVZ magmas, based on phenocryst assemblages. The techniques used for these determinations are outlined in Appendix A. No other estimates of pre-magmatic volatiles have been made for these magmas.

ANALYTICAL PROCEDURES

Samples

TVC and OVC tephra samples were collected in December and January, 1983/84, mainly from roadcuts in sections where exposure was good and a number of units could easily be identified. Samples generally contained pumice, lithic fragments, crystals and obsidian fragments. If the tephra unit contained a layer unusually rich in obsidian or crystals, that layer was individually sampled. Two to three kg. of bulk tephra were collected. Some samples of pure obsidian were hand picked from the outcrop. For thin tephra units (< 50 cm.), a single channel sample was taken, however, if the unit was over 50 cm. thick, samples were collected stratigraphically over approximatly 40 cm. intervals. Samples were dried, and stored in plastic bags. Sample locations and numbers are listed in Appendix C.

Sample Preparation

Obsidian and crystals were separated from bulk samples for volatile and temperature analyses. A portion of the bulk sample was sieved to remove the large pumice and fine dust, and an intermediate fraction (0.5 to 2 mm.) was used for hand picking obsidian and crystals.

Obsidian was found in most samples, although the abundance varied widely from unit to unit. The obsidian found in intermediate size fractions (0.5 to 2 mm.) was angular, blocky,

and transparent fragments, ranging in color from clear to black. Obsidian color was constant within some samples, but occasionally a complete spectrum was present. Thirty to one hundred fragments were removed from each bulk sample, depending on fragment size and obsidian abundance. About half of the grains were ground to approximately 75 mesh with an agate mortar and pestle, using acetone as a grinding solvent. The ground samples were dried overnight at 100 degrees C., and stored in glass vials for volatile analysis.

Crystals were also separated from the 0.5 to 2 mm. size fractions. Analyses of included magnetite-ilmenite grains were used to calculate temperature and oxygen fugacity (Buddington and Lindsley, 1964; Stormer, 1982), and glass inclusions were analysed to determine volatile contents. Initially, a hand magnet was run over the sample in order to separate plagioclase and mafic silicates with magnetite inclusions. This technique usually yielded a sufficient number of magnetite bearing mafic silicate crystals, and additional plagioclase was separated by hand picking. About 30-50 of each type of crystal were sorted. The crystals are generally euhedral, and some have glass adhered to the outside. Although they were not directly taken from the pumice, the crystals resemble those seen in pumice fragments, so are assumed to be derived from the magma. Most of the tephra units contained plagioclase, one or two mafic silicates, and magnetite-ilmenite pairs.

Polished thin sections were prepared of all obsidian and crystal samples for optical observation and electron microprobe analyses. Doubly polished chips of feldspar from a few samples were also made for high-temperature-stage measurements.

Petrographic Investigation

Obsidian grains from all samples were examined petrographically. In general, the grains show similar morphology: roughly equidimensional with angular or conchoidal boundaries. Within the grains, there is often a boxy fracture pattern, but this may have been caused by the grinding process during thin section preparation. No hydration rims were seen, and the birefringence pattern was not strained, suggesting that secondary hydration was not important. No other alteration, devitrification structures or large vesicles were observed. Phenocrysts of mafic silicates and feldspar were sometimes present in the glass.

Petrographic investigation shows that the color of obsidian fragments is controlled by microphenocrysts. Thin sections of dark and light glass picked from the same sample show distinct differences. Whereas the light glass is completely clear, the dark fragments contain a large number of tiny dark needlelike microphenocrysts. The exact composition of these phenocrysts is not certain, but they are probably plagioclase, because plagioclase is likely to be the first phase to crystallize. An

interesting feature of these microphenocrysts is that they show complex and variable flow patterns in the glass. The orientation of some microphenocrysts are completely random, but others show a pronounced lineation of the long axis, which seems to indicate that the glass was deforming soon before it quenched. The lineation is completely parallel in some samples, but is wavy or tightly folded in others, resembling flow banding in rhyolite lavavs. The lineation pattern is deflected around larger phenocrysts, indicating that the glass flowed around them. Immediately adjacent to the larger phenocrysts, there are generally fewer microphenocrysts, or an area of random orientation, possibly because the laminar flow was disrupted. Seen at high magnification, microphenocrysts in some grains seem to have very small particles adhered to them, which may be another phenocryst phase or small vesicles. The cooling in these grains may have been slightly slower than in the light grains, and the microphenocrysts may have provided nucleation centers for small crystals or bubbles of exsolving gas. These microphenocrysts, although not completely understood, may provide important information about the history of the obsidian fragments in which they are found.

Polished thin sections were prepared of crystal separates, but the relative percentages of crystals was not determined because the crystals sorted are not representative of true magmatic proportions. The types of crystals seen agree with those reported by other workers (Tables 1 and 2). The most

notable feature of the crystal populations of these tephras is that all of the youngest Taupo units (<20,000 yrs. B.P.), are pyroxene bearing and lack significant amphibole, whereas the older Taupo and all of the Okataina units contain amphibole. These mineralogies should reflect different water fugacities in the magma chamber at the time that the crystals were forming. Although compositional zonation of plagioclase has been reported (Ewart, 1963), no significant zonation was seen in crystals in these thin sections.

Magnetite and ilmenite grains are found in nearly equal abundance in mafic silicate and plagioclase separated from most tephra units. No oxidation exsolution lamelli or other evidence of alteration were seen in either oxide (Haggerty, 1976).

Glass inclusions are also present in most samples, mainly in the cores of mafic silicates. The inclusions range from 10 to 100 microns in diameter and are generally one phase, although some also contain a vapor bubble. The inclusions are mainly rounded blebs of glass, or negative crystal forms, but in some cases they are irregular shaped masses clinging to a magnetite or ilmenite crystal in a larger silicate grain. The number of inclusion-bearing grains varied from sample to sample, but did not seem to correlate with the number of inclusions in the grain itself. These glass inclusions are suitable for both electron microprobe and heating stage analysis.

Analytical Techniques

Water, sulfur and chlorine measurements, as well as temperature determinations were made on samples of most units.

Water contents of obsidian were determined using a Dupont Moisture Analyser, and by a Carl Fisher titration method, both at Sandia National Laboratories, Albuquerque, New Mexico (see Appendix D, part 1).

Sulfur and chlorine contents in obsidian and glass inclusions were analysed by electron microprobe at Victoria University of Wellington, New Zealand. Analytical details are given in Appendix D, part 2.

Temperatures within the magma chamber were determined by two techniques; Fe-Ti oxide equilibration geothermometry (Buddington and Lindsley, 1964; Stormer, 1983), and a less common technique, melt inclusion geothermometry (Roedder, 1984).

Magnetite and ilmenite were analysed by electron microprobe at the University of New Mexico, Albuquerque, New Mexico. Many silicate phenocrysts from Taupo and Okataina tephra contain blebs of magnetite and ilmenite which were trapped during growth in the magma chamber. These two oxide phases should be in equilibrium because they were growing at the same time. Therefore, they should be ideal for iron-titanium oxide geothermometry as described by Buddington and Lindsley (1964). The method used for these analyses is described in Appendix D, part 3.

The second method for determining magmatic temperature of rhyolites is an experimental technique whereby the temperatures at which glass inclusions within magmatic phenocrysts melted was determined by heating measurements made with a Linkham 1500 heating stage at New Mexico Institute of Mining and Technology, Socorro, New Mexico. Melt inclusion temperatures were only determined for one sample, from the Hatepe plinian eruption. The method used for these analyses is in Appendix D, part 4.

Two main parameters can be determined from glass inclusions: melting and homogenization temperatures. Melting temperature is the most straightforward theoretically, indicating the minimum temperature at which the magma would have been molten (Roedder, 1984). In practice, however, it is often difficult to determine melting temperatures because the appearance of the inclusion glass does not change during or after the melting. In this case, melting was detected by movement or change in shape of the vapor bubble, sudden vesiculation of one or more bubbles, or movement of glass into cracks in the host mineral.

The second parameter, homogenization temperature, is easier to determine experimentally, but the meaning of these values is not well understood. This temperature, at which all phases of an inclusion homogenize to a single phase, usually vapor and glass becoming all glass, should indicate the minimum temperature at which the material was trapped, and therefore the minimum temperature at which the host phase grew (Roedder, 1984). The

pressure at which the melt inclusion was trapped will have a significant effect on the homogenization temperature, and must be taken into account when interpreting results.

RESULTS

Water

Water contents of obsidian in tephra varies from 0.3 to 4.1 wt.% (see Tables 3 and 4). Values of over 2.5 wt.% are only seen in a few samples, and are probably caused by hydration. Repeat analyses of obsidian from a dome related flow consistently gave water content of 0.1 wt.%.

The Dupont Moisture analyser method does not give any information about water content variation between different fragments of obsidian because a number of fragments must be crushed together for each analysis. However, the Karl Fisher titration method does allow analyses of individual pieces of obsidian. Preliminary analyses by this technique show that water contents of most fragments agree to within 0.2 wt % of the value of the crushed sample (representing an average of a number of grains), but that some fragments vary by an average of 0.5 wt % from this value. One set of individual fragment analyses done by Karl Fisher titration are shown in Table 5. Other Karl Fisher analyses are listed in Appendix D-1.

Chlorine

The Cl values for obsidian range between 1200 and 1700 ppm, whereas glass inclusion values are between 1750 and 2000 ppm (Table 6). Numerous glass inclusions and obsidian fragments could be analysed in each sample, so homogeneity could be evaluated (Table 7). Different analyses of the same sample are

Table 3. Water contents of obsidian in tephra deposits from the Taupo Volcanic Center tephra.

Unit	Age (x1000 yrs)	sample number	stratigraphic position	water content (%)
Taupo Plinian	2	83-016	top	0.49
" "	"	83-015	inter	0.24
" "	"	83-014	base	0.14
" "	"	83-022		0.38
Rotongaio	2	83-041	-	0.60
Hatepe phreato.	2	83-005	top	1.07
" "	"	83-023	inter	1.60
" "	"	83-004	inter	1.55
" "	"	83-006	inter	1.59
" "	"	83-003	inter	0.58
" "	"	83-002	base	0.42
Hatepe plinian	2	83-007	-	0.46
" "	"	83-027	-	0.42
" "	"	83-045	-	0.62
Initial Ash	2	83-044	top	0.30
" "	"	83-043	base	0.46
Marapa	2.2	83-026	top	1.20
" "	"	83-025	inter	0.89
" "	"	83-024	base	0.79
Whaikapu	2.8	83-029	-	1.64
Waihimia	3.2	83-018	base	1.11
Motutere	5.4	83-008	-	1.60
Opepe	8.8	83-030	top	1.16
" "	"	83-031	inter	1.41
" "	"	83-032	base	1.44
Porunui	9.5	83-009	-	0.90
Karapiti	9.8	83-012	top	1.23
" "	"	83-011	inter	1.40
" "	"	83-034	top	1.56
Oruanui	20	83-051	-	4.07
" "	"	83-050	-	1.37
" "	"	83-082	-	1.28
Okaia	22	83-047	-	1.09

Tihoi	38	83-055	-	2.61

Table 4. Water contents of obsidian in Okataina Volcanic Center tephra.

Unit	Age (x 1000 yrs)	Sample Number	Stratigraphic Postion	Water Content (%)
Kaharoa	0.65-0.93	83-080	-	0.60
Whakatani	5	83-068	-	0.86
Mamaku	7	83-066	top	0.93
" "	"	83-065	base	0.98
Rotoma	9	83-064	top	0.83
" "	"	83-063	inter	0.81
" "	"	83-062	base	0.80
Rotorua	13	83-091	top	0.64
" "	"	83-088	inter	0.63
" "	"	83-083	inter	1.23
" "	"	83-085	inter	1.41
" "	"	83-087	inter	1.22
" "	"	83-086	base	1.28
Rerewhakaaipu	14.7	83-079	top	0.68
" "	"	83-078	base	1.30
Okareka	17	83-076	top	0.90
Terere	19	83-060	top	0.87
" "	"	83-059	inter	0.61
" "	"	83-057	base	0.78
Omateroa	28	83-074	-	2.17
Awakeri	30	83-072	-	1.43
Mangaone	31	83-071	top	1.68
" "	"	83-071	base	1.52

Table 5. Variation between different obsidian fragments from sample 83-011 (Karapiti). Analysed by Karl Fisher titration.

Analysis Number	Sample Weight	description of fragment	water content (wt.%)
1-5	0.0103	one grey fragment	0.95
1-6	0.0267	one grey fragment	0.82
1-7	0.0256	one dark grey fragment	1.35
1-8	0.0390	one large black fragment	0.78
1-10	0.0156	one black fragment	1.29
1-12	0.0192	one black fragment	1.29
1-13	0.0262	one grey fragment	1.09
		mean:	1.08
		standard deviation:	0.23
		co-efficient of variation:	21%

The water content determined by Karl-Fisher titrometry for a crushed sample of many obsidian fragments, is 1.16 wt.%. This should represent an average value for obsidian fragments, and it agrees well with the determined average for these seven fragments.

Table 6. Chlorine content of obsidian and glass inclusions for the Taupo and Okataina center eruptions.

Unit	Sample Number	Obsidian n	Obsidian Cl wt. %	Obsidian SD	Glass Incl. n	Glass Incl. Cl wt. %	Glass Incl. SD
Taupo Volcanic Center							
Taupo Plinian	83-015	4	0.140	0.007	6	0.178	0.006
Hatepe Phreat.	83-003	8	0.131	0.008	4	0.17	0.007
Hatepe Plin.	83-027	11	0.121	0.020	2	0.173	0.005
	83-045	4	0.120	0.005		-	-
Marapa	83-025	6	0.136	0.006	6	0.188	0.009
Whaikapu	83-029	5	0.160	0.012	4	0.184	0.006
Waihimia	83-020	9	0.129	0.011	4	0.183	0.003
Motutere	83-008	3	0.157	0.006	7	0.197	0.013
Opepe	83-032	9	0.141	0.018	8	0.181	0.009
Porunui	83-009	7	0.143	0.013	6	0.186	0.015
Karapiti	83-011	5	0.138	0.016	4	0.190	0.012
Oruanui	83-050	4	0.153	0.015	6	0.234	0.024
Okaia	83-047		-	-	8	0.211	0.024
Tihoi	83-054		-	-	8	0.224	0.034
Okataina Volcanic Center							
Kaharoa	83-080		-	-	3	0.198	0.001
Whakatani	83-068	6	0.159	0.011	5	0.176	0.011
Mamaku	83-066	7	0.149	0.014	4	0.192	0.009
Rotoma	83-064	10	0.162	0.014	3	0.196	0.006
Waiohau	83-081		-	-	6	0.200	0.012
Rotorua	83-085	3	0.168	0.004	5	0.173	0.007
Okareka	83-076	3	0.128	0.006		-	-
Terere	83-060	6	0.119	0.007	1	0.195	

Omateroa	83-075	3	0.137	0.001		-	-
Awakeri	83-072	3	0.155	0.006	4	0.189	0.060
Mangaone	83-071	10	0.141	0.020	2	0.132	

n = number of analyses included in the average wt.% Cl.
SD = standard deviation

Table 7. Variation in chlorine content between and within 3 obsidian grains from the Rotoma unit (83-064)

Grain Variation	Chlorine Content	Part of Grain	Mean for Grain	S.D.	Coefficient of Variation
A	0.149				
A	0.165		0.163	±0.013	8%
A	0.174				
B	0.179	edge			
B	0.157				
B	0.138		0.159	±0.017	11%
B	0.160	center			
C	0.149	edge			
C	0.170		0.166	±0.016	9%
C	0.180	center			

usually within 10% of each other, and there is no systematic variation from center to edge of the obsidian fragment.

Iron-Titanium oxides

Magmatic temperatures determined from magnetite-ilmenite equilibrium range between 730 and 930° C, with log fO_2 values between -15 and -11. Results of these analyses are compiled in Tables 8 and 9. Chemical analyses of the magnetite and ilmenite grains are listed in Table D-3-1 (Appendix D-3).

Glass Inclusions

Glass inclusions in plagioclase phenocrysts were analysed in tephra from the Hatepe plinian eruption. Homogenization temperatures were not attainable on a stage which reached 1000 degrees C. Melt temperatures are shown in Table 10.

Table 8. Temperature/Oxygen fugacity values for Taupo center tephras. Each grain (A,B,C,D) is a silicate phenocryst containing a number of magnetite and ilmenite inclusions. The temperature and oxygen fugacity are determined from the average of magnetite and ilmenite composition from each grain, using a method described by Stormer, (1983).

Unit	grain	temperature (degrees C)	oxygen fugacity $\log fO_2$
Taupo Plin. (017)	A	904±29	-11.7±0.3
	B	918±28	-11.3±0.3
	C	907±29	-11.6±0.3
Hatepe Plin. (027)	A	809±34	-13.9±0.5
	B	790±52	-14.5±0.9
	C	819±33	-13.6±0.5
Initial Ash (044)	A	826±32	-13.3±0.4
	B	824±31	-13.3±0.4
	C	846±29	-12.7±0.4
Marapa (025)	A	827±33	-13.4±0.4
	B	838±32	-13.9±0.4
Waikapu (029)	A	828±35	-13.6±0.5
	B	840±35	-13.3±0.5
Waihimia (020)	A	788±53	-14.5±0.9
	C	806±36	-14.1±0.5
Motutere (008)	A	804±35	-14.0±0.5
	B	852±31	-12.8±0.4
	C	816±34	-13.7±0.5
	D	854±32	-12.8±0.4
Opepe (031)	A	848±33	-13.0±0.4
	B	855±31	-12.7±0.4
	C	817±33	-13.6±0.5
	D	849±32	-13.0±0.4
Porunui (009)	A	864±31	-12.5±0.4
	B	833±35	-13.5±0.5
	C	834±34	-13.4±0.5
	D	875±31	-12.3±0.4
Karapiti (010)	A	819±35	-13.7±0.5
	B	798±52	-14.2±0.9
	C	818±36	-13.8±0.5
Oruanui (050)	A	745±42	-15.2±0.7
	B	770±38	-14.1±0.5

Table 9 . Temperature/Oxygen fugacity values for Okataina center tephras. Each grain (A,B,C,D), is a silicate phenocryst containing a number of magnetite and ilmenite inclusions. The temperature and oxygen fugacity are determined from the average of magnetite and ilmenite conpositions from each grain, using a method described by Stormer (1983).

Unit	grain	temperature (degrees C)	oxygen fugacity $\log fO_2$
Kaharoa (080)	A	833±25	-12.4±0.3
	B	793±36	-13.2±0.5
Whakatani (068)	A	781±36	-13.5±0.5
	B	793±36	-13.0±0.4
	C	773±37	-13.7±0.5
	D	807±26	-12.9±0.3
Mamaku (066)	A	788±36	-13.1±0.4
	B	781±36	-13.6±0.5
	C	804±25	-12.8±0.3
	D	811±24	-12.5±0.3
Rotoma (064)	A	762±41	-12.9±0.5
	B	786±36	-13.1±0.4
	C	797±36	-12.7±0.4
	D	814±24	-12.4±0.3
Waiohau (081)	A	791±36	-13.1±0.4
	B	795±36	-12.8±0.4
	C	797±35	-12.8±0.4
Rotorua (085)	A	866±22	-11.3±0.2
	B	856±23	-11.5±0.2
	C	853±23	-11.5±0.2
Terere (059)	A	806±25	-12.6±0.3
	B	796±36	-12.8±0.4
	C	782±37	-13.3±0.5
Awakeri (072)	A	810±25	-12.7±0.3
	B	808±26	-12.8±0.3
	C	819±25	-12.5±0.3
Mangaone (071)	A	829±23	-12.0±0.3
	B	829±24	-12.2±0.3
	C	843±23	-11.8±0.2

	C	765±38	-14.1±0.5
	D	787±39	-13.9±0.6
Okaia	A	743±40	-15.1±0.6
(047)	B	773±38	-14.1±0.6
	C	802±26	-13.0±0.3
Tihoi	A	785±38	-13.9±0.6
(054)	C	729±41	-15.4±0.7

Table 10. Glass inclusion geothermometry. All analyses on plagioclase from the Hatepe Plinian eruption, sample (83-027).

Inclusion	Melt Temperature (degrees C)	Decrepitation Temperature (degrees C)
1	740	850
2	600*	-
3	700	800
4	700	-

*Determined from very slight bubble movement.

DISCUSSION

Volatiles in Obsidian

Two important questions must be examined before evaluating the H_2O contents of obsidian. First, is the obsidian is actual juvenile material, and second, is the analysed water magmatically derived, as suggested by Eichelberger and Westrich (1981). Alternative possibilities can be considered for the derivation of the obsidian and the water contained in the obsidian.

The obsidian could be lithic material derived from dome or flow material near the vent which is shattered during the explosive eruption and incorporated into the plinian eruption column. If this were the case, the obsidian should contain approximately 0.1 to 0.2 wt.% H_2O, which is the atmospheric equilibration value of water in rhyolitic melts, the value indicative of degassed dome material (Taylor et. al., 1983). An analysed TVZ dome sample (DOBS), contains 0.1 wt.% H_2O. Lithic material which has not been hydrated can therefore be distinguished from primary material by the low water content. As shown in Fig. 4, only a few samples contain less than 0.3 wt.% H_2O. These samples, mostly from the Taupo and Hatepe plinian eruptions, could be either flow derived or highly degassed plinian material.

The water in an obsidian fragment may also have been introduced by progressive, post-eruption hydration, rather than being magmatically derived. If this were the case, the water content would increase steadily over time, but this trend is not

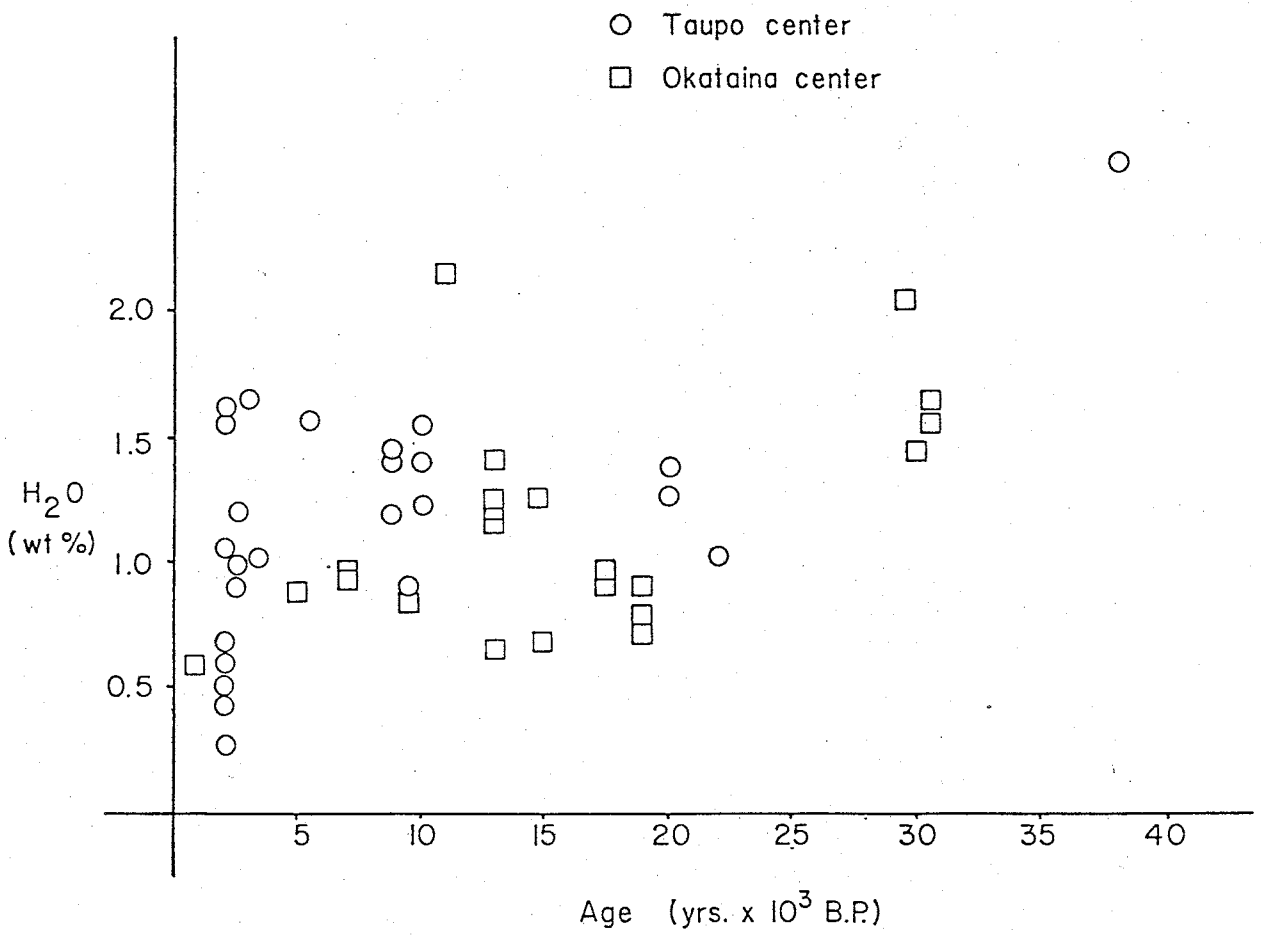

Figure 4. Weight percent H_2O in obsidian versus age for Taupo and Okataina tephra.

Sample 051, which contains 4.2 wt.% H_2O, is obviously hydrated, and is not included in this graph.

seen in deposits less than 20,000 yrs. old, when hydration apparently became a factor (Fig. 4). One anomalous obsidian sample in the Oruanui plinian (83-051), contains 4.2 wt.% H_2O, and the individual obsidian fragments are multicolored (red, green, brown), opaque and have a sugary appearance. This is the only sample in which this type of obsidian was observed. Hydrated obsidian can also be positively identified by its delta D value, which will reflect the local meteoric water.

Based on the considerations above, I suggest that most obsidian from TVC and OVC tephra are primary and represent quenched samples of the magma which have not been altered by hydration.

A graphical representation of water contents of different eruptions, and of different stratigraphic intervals within one eruption is presented in Fig. 5. The water contents of obsidian from different stratigraphic intervals of one eruptions are variable, but do not show any consistent stratigraphic trends within individual units. There is also variation in water contents from eruption to eruption. These data suggest that the obsidian have degassed to varying degrees during eruption, and do not contain their initial total magmatic water content.

Cl content does not vary systematically with age. (Fig. 6) This observations suggest that the Cl is magmatically derived, because if it were secondary there should be an increase in Cl with age, analagous to water increase with hydration. Also, the Cl contents are uniform from the center ot the edge of obsidian

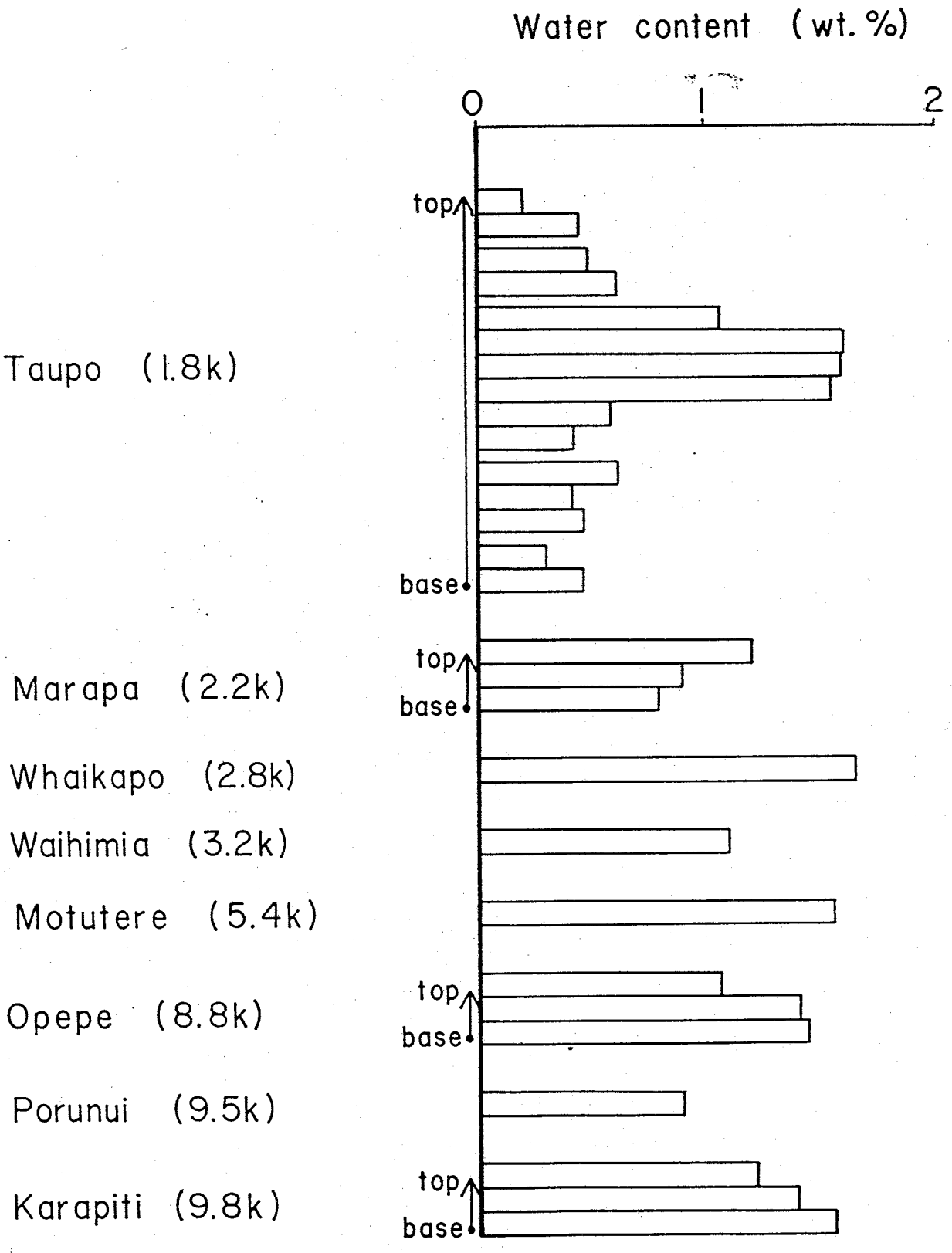

Figure 5. Water content in obsidian from different Taupo center eruptions and different stratigraphic positions within one eruption.

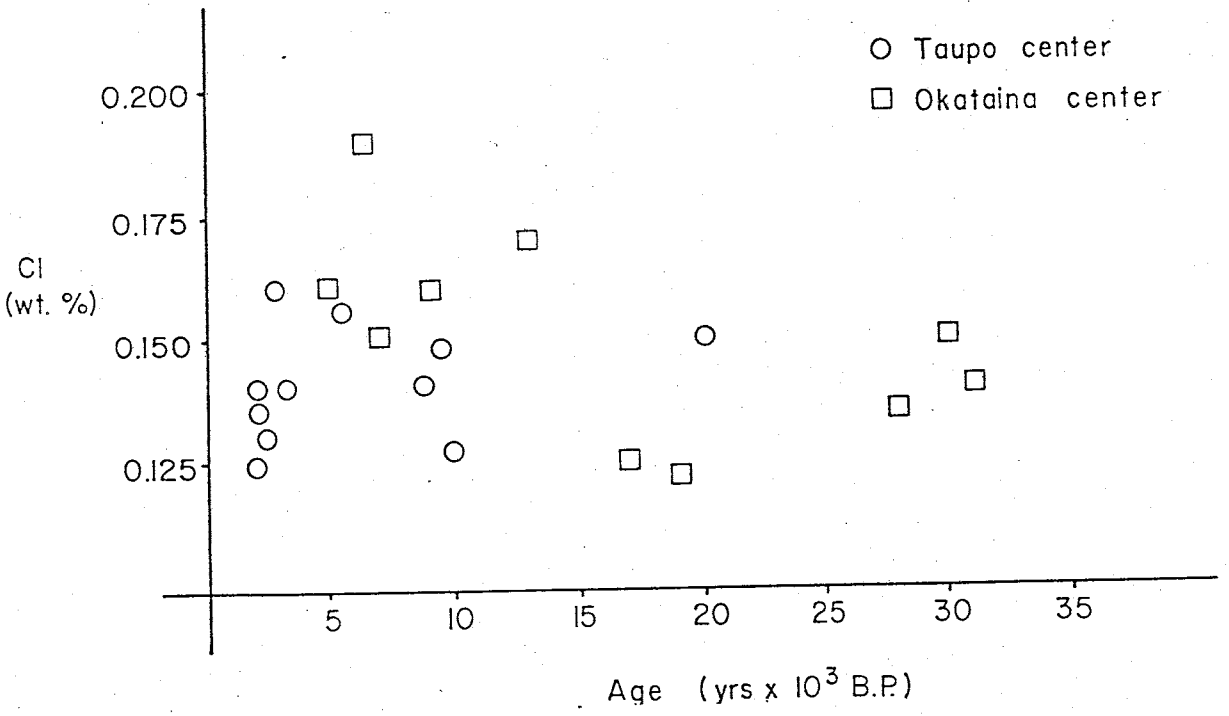

Fig. 6. Weight percent Cl in obsidian versus age for Taupo and Okataina center tephras.

grains, which suggests that Cl is not being introduced after the eruption. The Cl shows variations between units, but no information about stratigraphic variation within one unit is known. These chlorine values are consistently lower than chlorine in glass inclusions from the same sample which supports the idea that the obsidians represent magmatic material which has lost a certain percentage of volatiles before quenching (Fig. 7).

Both H_2O and Cl seem to have partially exsolved before they were trapped as the magma quenched to obsidian. This theory is strengthened when values of H_2O and Cl in obsidian are compared (Fig. 8). These two components show a visible correlation (r^2 = .5), which suggests that they were degassed at roughly the same rate as the magma was erupted. This is conclusion implies that Cl and H_2O have similar solubility mechanisms, and could help model Cl behavior in an igneous melt. The water analyses in Fig. 8 are partly from Dupont Moisture Analyser and partly from Karl Fisher titration analysis.

Volatiles in Glass Inclusions

Although glass inclusions trap pristine magma, a number of factors can cause glass inclusions to change major or volatile element chemistry subsequent to entrapment in the growing crystal.

If the crystal and melt inclusion are held at a temperature below the crystallization point of the mineral, but higher than the quench point of the glass, additional mineral may be

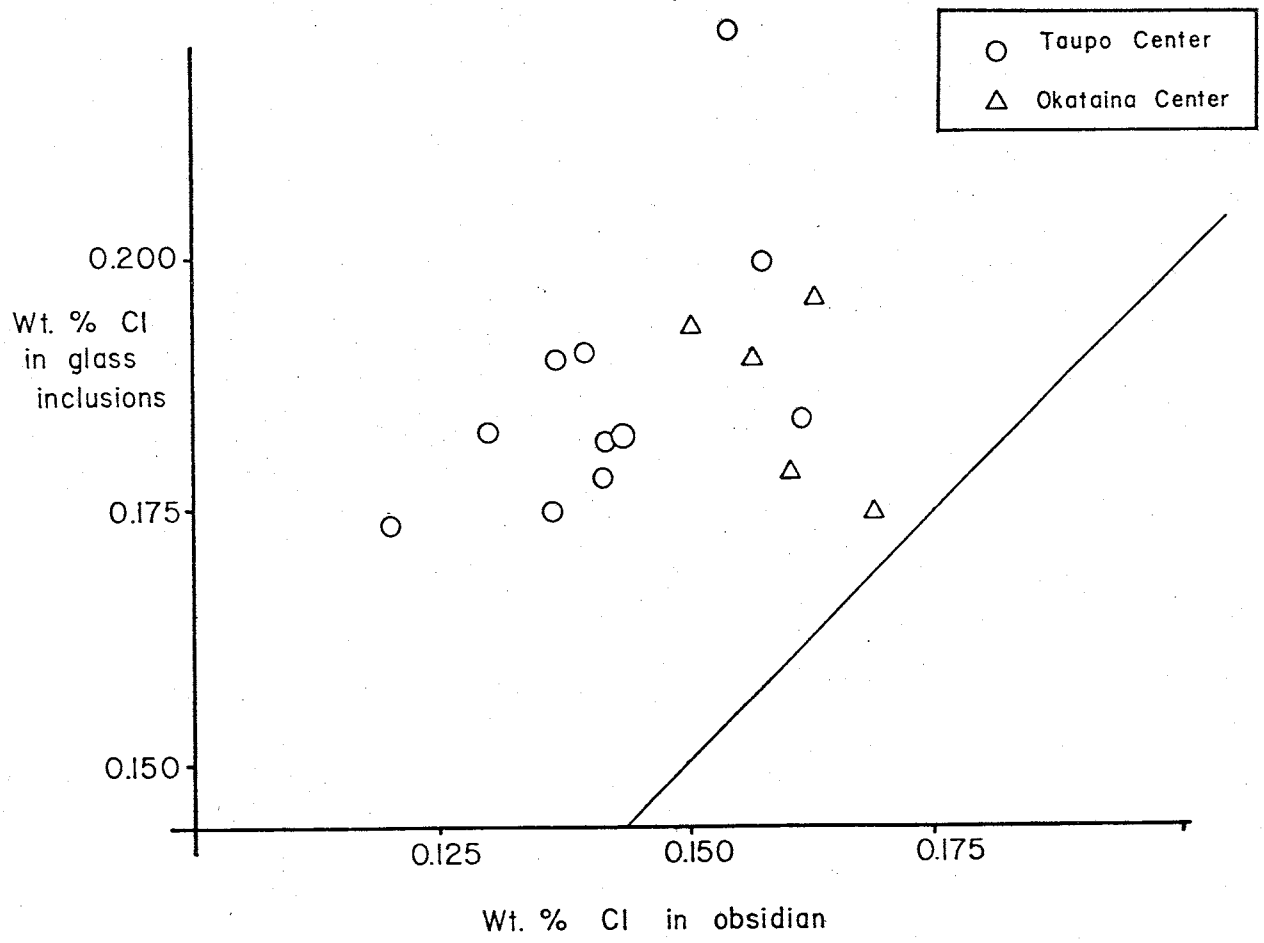

Figure 7. Weight percent Cl in glass inclusions versus obsidian. The oblique line represents a 1:1 correlation between Cl in glass inclusions and obsidian.

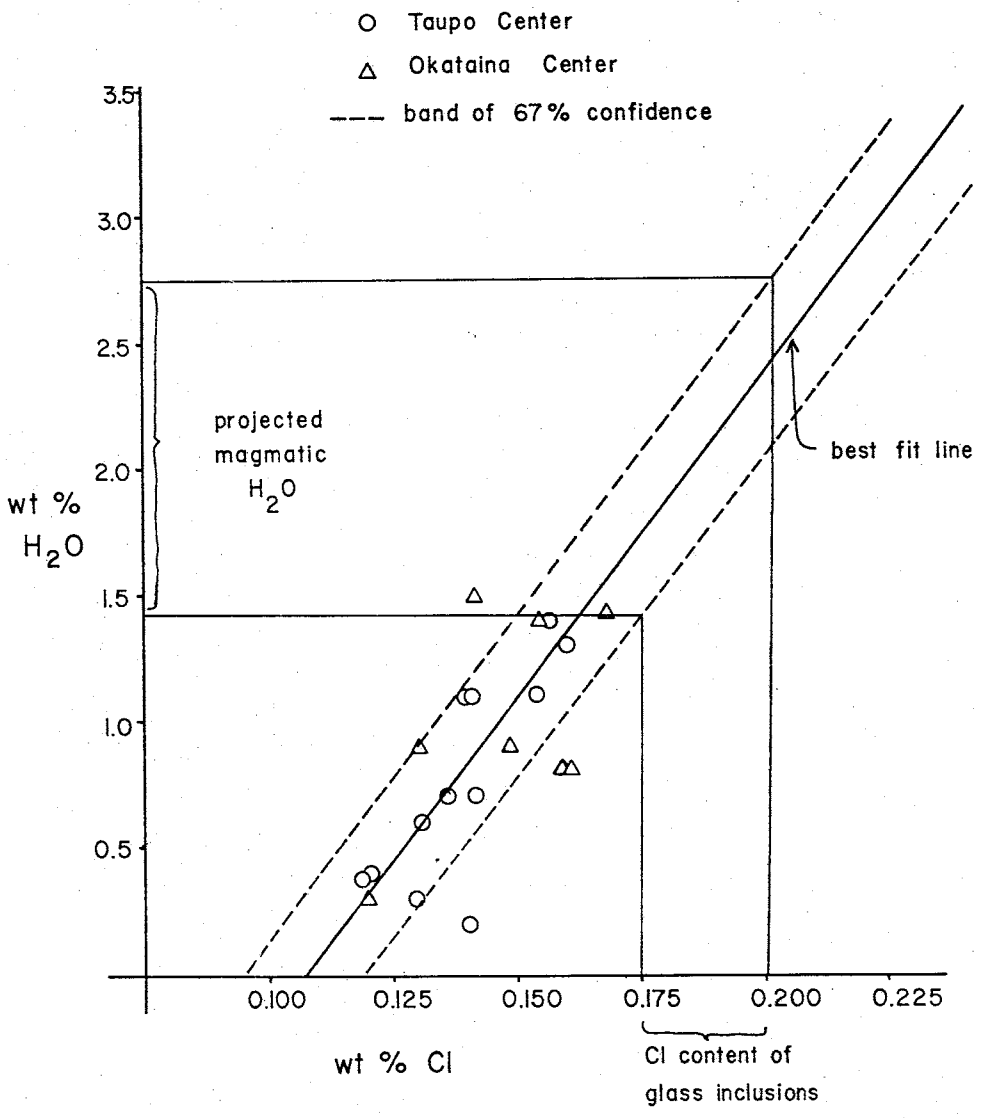
Taupo Center
Okataina Center
band of 67% confidence
3.5
3.0
2.5
2.0
1.5
1.0
0.5
wt % H_2O
projected magmatic H_2O
best fit line
0.100
0.125
0.150
0.175
0.200
0.225
wt % Cl
Cl content of glass inclusions

deposited on the walls of the inclusion. Elements which are not included in the crystal structure would be concentrated in the glass inclusions. Watson (1976) saw this effect in basaltic phenocrysts, where the major element chemistry of glass inclusions in olivine, pyroxene, and plagioclase were quite different, and were consistent with post-entrapment deposition of the host crystal. Volatiles can be concentrated in inclusion glass by this process.

Magmatic volatile contents in inclusions can also be modified by the growth of a vapor bubble during slow cooling (Roedder, 1976). At reduced pressure and temperature, the vapor will partition into a bubble, and the remaining glass will be slightly degassed. No quantitative studies have been made of this effect.

These effects, however, are all minimized in products of explosive eruptions, where crystals grow and quench rapidly (Roedder, 1984). No compositional gradients are seen at inclusion/crystal boundaries in phenocrysts from the explosive Toba eruption, and glass inclusions have the same major element chemistry as the matrix glass (Beddoe-Stephens et. al., 1983). This indicates that no host crystal was deposited on the walls of the inclusion. Most TVZ phenocrysts, especially pyroxenes, appear to have grown quickly, because they contain large concentrations of glass inclusions in their cores (Roedder, 1976), and may have quenched quickly because few have vapor bubbles (Roedder, 1984). For these reasons, the Taupo glass

inclusions are probably quite close to early magmatic composition. The glass inclusions and obsidian from these deposits are chemically similar, based in electron microprobe analyses (Table 11). This information suggests that the glass inclusions are close to magmatic composition.

The values for Cl in TVZ magmas, based on glass inclusions data, are between 1750 and 2000 ppm, which are consistent with Cl analyses in glass inclusions from other tephras (Devine et. al., 1984). TVZ sulfur values of less than 150 ppm are also in agreement with data presented by Devine et. al., which show that, as silica content increases, S content decreases.

Comparison of these volatile contents of glass inclusions with values of degassed material (pumice or matrix glass), will yield an estimate of the atmospheric input of that volatile, if the volume of the eruption is known. Devine et. al. (1984), used this technique to calculate atmospheric input of S and Cl for a number of large volcanic eruptions. For the Taupo, although the volatile values for fully degassed pumice are not known, partial atmospheric imput of the different eruptions can be determined by comparing Cl values of obsidian and glass inclusions (Tables 11 and 12). The method used involves converting the volume (km^3) of tephra to mass, and then determining the mass of Cl output based on the weight percent of Cl difference between obsidian and glass inclusions. The specific equations are as follows:

Vol. of tephra (km^3)/3 = Dense Rock Equivalent (DRE) (km^3)

DRE(km^3) x 2.5 x 10^{12} kg/km^3 = mass of deposit (kg)

[(wt.% Cl output) x (mass of deposit)]/100 =

total Cl output (kg)

These values are not considered entirely accurate, because the obsidian is only partially degassed, but at least give an idea of the order of magnitude of Cl which was contributed to the atmosphere. The atmospheric input of Cl varies between 0.16×10^{12} to 47.8×10^{12} grams per eruption.

Table 11. Representative microprobe analysis of obsidian and inclusion glass from the Taupo plinian (sample 015).

Oxide	Obsidian Wt.%	Inclusion Glass Wt.%
SiO_2	74.8	74.1
TiO_2	0.3	0.3
Al_2O_3	12.6	12.7
FeO	1.9	2.0
MgO	0.2	0.2
CaO	1.3	1.2
Na_2O	4.2	3.8
K_2O	2.9	2.8
total	98.4	97.5

Table 12. Atmospheric input of Cl for eruptions of the Taupo Ceenter based on eruptive volumes shown in Table 1.

Unit	Cl difference between obs. and glass incl. (wt%)	Total Chlorine Emission (gr.x 10^{12})* 1	2	3	4
Taupo Plinian	0.038	3.90	3.85	-	7.62
Hatepe Phreato.	0.044	1.22	-	-	-
Hatepe Plin.	0.053	2.08	0.80	-	2.65
Marapa	0.052	-	0.86	0.28	-
Whaikapu	0.024	-	0.30	0.16	-
Waihimia	0.054	-	6.30	6.75	13.05
Motutere	0.040	-	0.17	-	-
Opepe	0.041	-	1.37	1.71	-
Porunui	0.043	-	1.08	1.25	-
Karapiti	0.052	-	0.87	2.17	-
Oruanui	0.082	-	47.80	-	-

*Based on volume estimates given by:
1 = Froggatt, 1981
2 = Froggatt, 1982
3 = Vucetich and Pullar, 1973
4 = Walker, 1980

Table 13. Atmospheric input of Cl for eruptions of the Okataina Center based on eruptive volumes shown in table 1.

Unit	Cl difference between obs. and glass incl. (wt%)	Total Chlorine Emission (gr x 10^{12})* 1	2
Whakatani	0.017	0.85	1.42
Mamaku	0.043	2.15	-
Rotoma	0.033	3.30	3.30
Rotarua	0.005	0.29	-
Terere	0.076	5.70	-
Awakeri	0.034	0.57	0.57

*Based on volume estimates by:
1 = Froggatt, 1982
2 = Nairn, 1980

Temperature Determinations

The temperatures determined by Fe-Ti oxide equlibria, are reasonable magmatic values, ranging from 730 to 930°C. These values agree with those determined by other workers for some Taupo and Okataina tephras (Ewart et. al., 1975; Howorth, 1979). Three different buffer trends are apparent in Fig. 9, one for the Okataina center tephras, one for Taupo tephras older than 20,000 yrs. BP, and a third for Taupo tephras younger than 20,000 yrs. BP.

The different temperature/oxygen fugacity trends seem to reflect major differences in the magmas producing Taupo and Okataina tephras. The Okataina center magma has been on a distinctly different buffer trend than the Taupo, but remained constant throughout time, showing a magma chamber which has been stable. The Taupo center, on the other hand, shows a distinct change at 20,000 yrs. B.P., from magmatic conditions similar to those of the Okataina center, to higher temperature, lower oxygen fugacity conditions. This change must be due to a major reinjection of magma following the very voluminous Oruanui and related eruptions, which produced 310 km^3 of ejecta (Wilson et. al., 1984).

The shift in the temperature/oxygen fugacity data from older to younger Taupo material coincides with a change in dominant mafic silicate mineralogy from amphibole to pyroxene. Tephra from the Okataina center, whose buffer trend is close to that for older Taupo material, also contains amphibole. This suggests

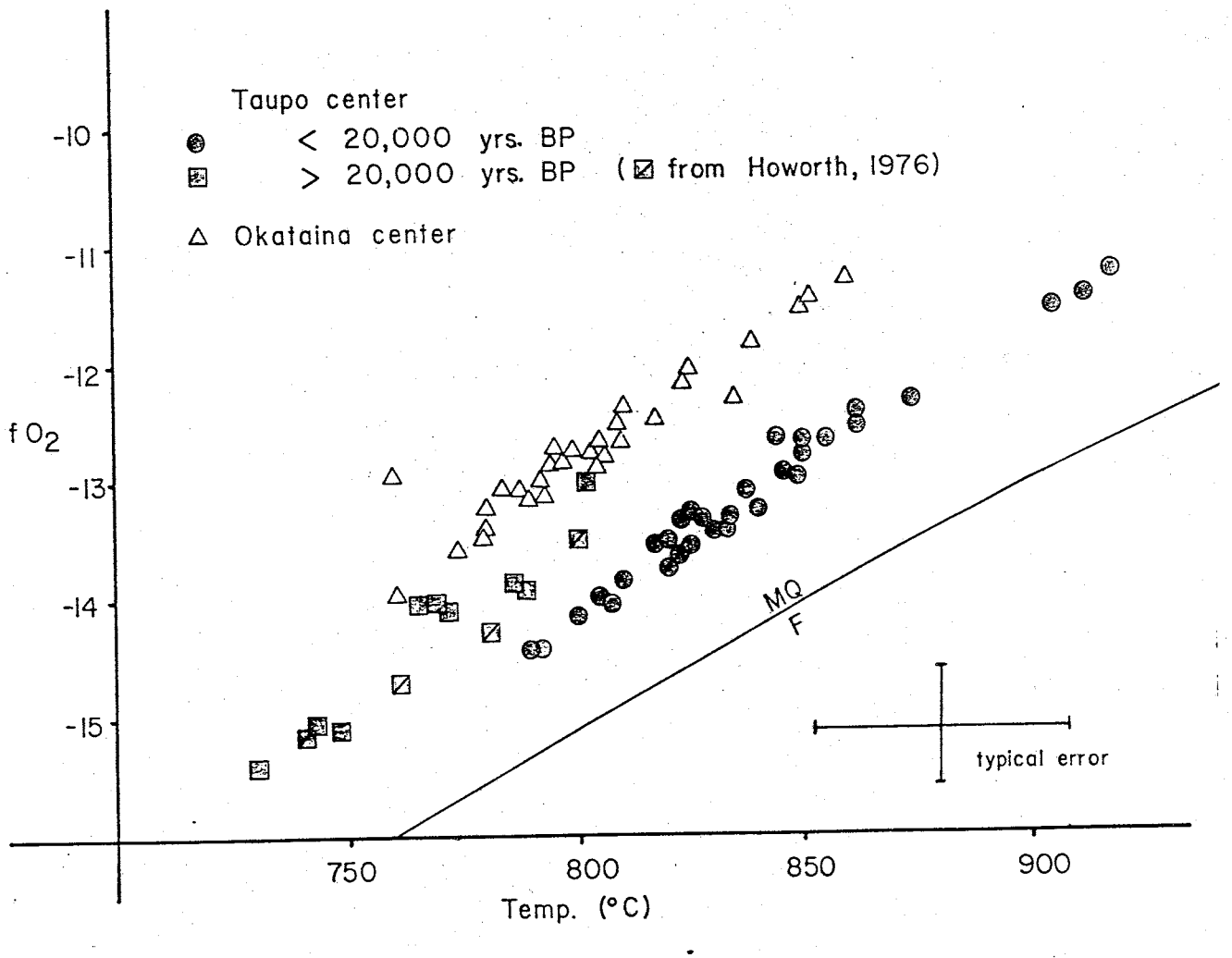

Figure 9. Temperature and oxygen fugacity values for Taupo and Okataina center tephras. Temperature and oxygen fugacity values from Howorth (1976) are not recalculated.

that the higher oxygen-fugacity buffer trends represent a higher water content in the parent magma, thereby producing hydrous rather than anhydrous mafic silicates from magma of the same initial chemical composition.

Another conclusion from the pre-magmatic temperature determinations is that the highly explosive Taupo plinian eruption magma appears to be about 50-100 degrees hotter than the average, and about 35 degrees hotter than the next hottest magmatic temperature. Although no precise mechanisms are suggested here, this high temperature may be related to the high degree of explosivity shown by this eruption.

The glass-inclusion melt-temperature determinations for the Hatepe plinian seem reasonable in view of the magnetite-ilmenite temperatures, which were around 800^{o}C. The melt temperatures determined by fluid inclusions should be somewhat lower than magmatic temperatures determined by Fe-Ti oxides, because the magma was still above the quench point of glass when these oxide minerals formed.

As mentioned before, homogenization of glass inclusions was not attainable. At 1000^{o}C, the inclusions were still exsolving rather than dissolving volatiles, as shown by bubble size increase. This expansion of the vapor bubble is probably caused by stretching of the host crystal due to glass expansion. Several inclusions decrepitated at about 800^{o}C, causing the host crystal to shatter, allowing glass to escape along fractures.

This behavior suggests that these inclusions were trapped in a system with high confining pressure, sufficient to allow glass to deform or rupture its host crystal when reheated to magmatic temperature. The simultaneous nucleation and growth of many small bubbles seen in several inclusions, suggests that the glass is volatile rich, although this relationship has not been quantified.

Volatile Content of TVZ Magma Chamber

The wide range of water contents seen in TVZ obsidian suggests that degassing of this material occurs prior to quenching. The water, therefore, is probably not representative of total magmatic water contents. The least degassed sample of obsidian, which contains 2.5 wt.% H_2O, may be approaching a true magmatic water value, based on conclusions by Taylor et. al. (1983), from work on obsidian from Long Valley, California.

Taylor et. al. (1983) noted water variations similar to those observed from Taupo, but also noticed that the deuterium content of the water varied proportionally with the percent of trapped water. From this, they concluded that as the magma degassed, deuterium and hydrogen isotopes were fractionated, and therefore the amount of water quenched in the obsidian is related to the isotopic signature (Fig. 10). From this data, they also predict that obsidian showing magmatic isotopic delta D values of between -60 and -70 permil would contain pre-eruptive water contents. These values range between about 2.5 and 3.0 wt.% H_2O.

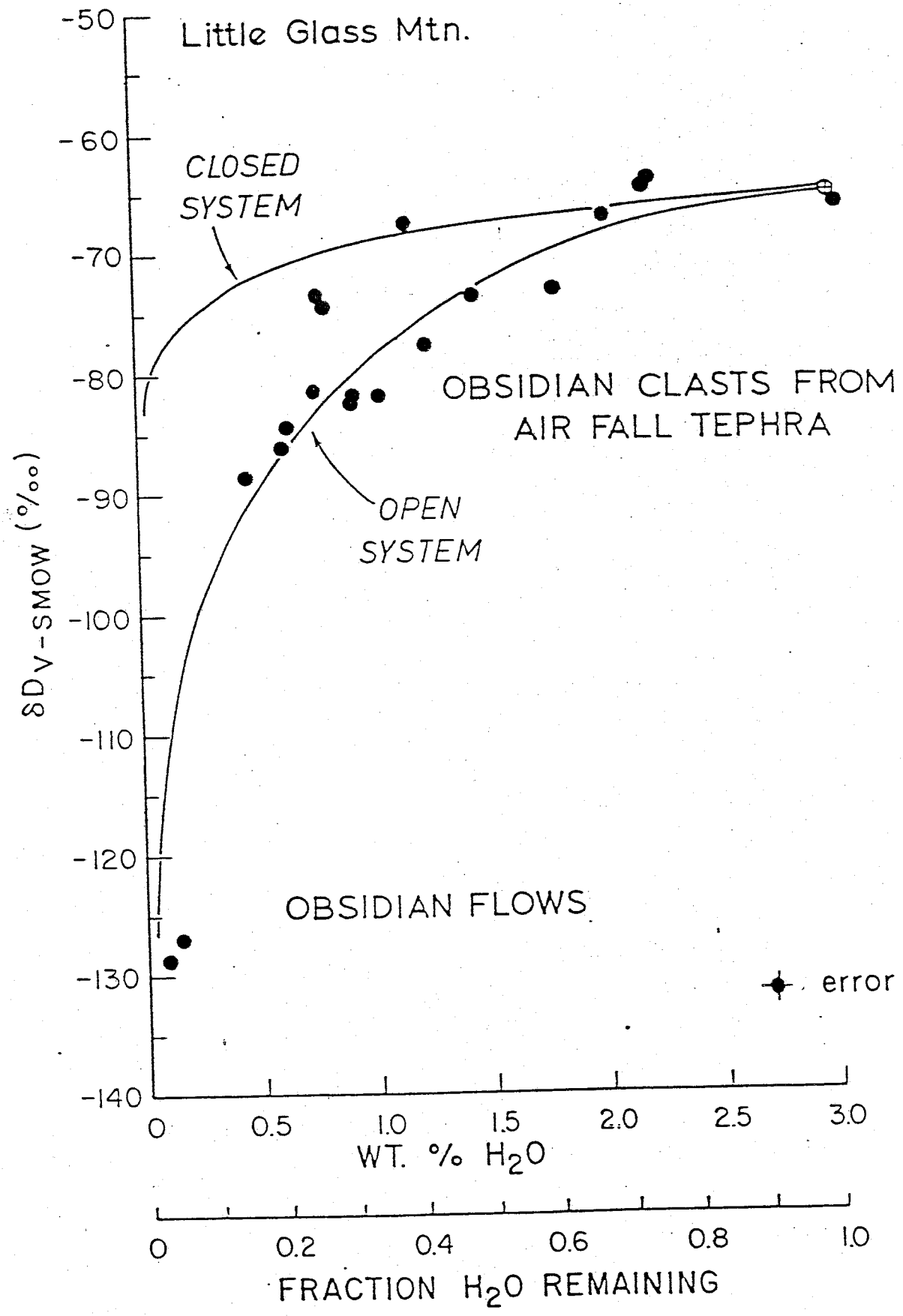

Figure 10. Delta D versus H_2O for obsidian from Long Valley, California.

From Taylor, 1983

One preliminary analysis of delta D of Taupo obsidian gives a value of -70 permil at 1.6 wt.% H_2O, which is fairly consistent with the trend shown by Taylor et. al. (1983). The next step in the study of the degassing history of obsidian from the TVZ will be to analyse the delta D values for all tephra units from the TVC and OVC, which will add significance to the water contents.

A second estimate of pre-magmatic water content is based on the correlation between H_2O and Cl in obsidians, and the magmatic Cl values from glass inclusions. If the calculated correlation line (Fig. 8) is extended to chlorine contents similar to those from the glass inclusions, water content in the glass inclusions, representing the original magma, could be predicted. Using a correlation band with a 67% confidence limit, and glass inclusion Cl content of 1750 and 2000 ppm, original water contents between 1.5 and 2.75 wt.% are predicted. This estimate is slightly lower than values from Taylor et. al., (1983).

These magmatic water content estimates do not agree with values determined from theoretical solubility of H_2O or mineral equilibria studies. Ewart et. al. (1975) estimated a magmatic water content of between 4 and 8 wt.%, based on phenocryst equilibria, and also concluded that the magma was saturated with water. A calculated value for the saturation of water in a magma chamber for a TVZ rhyolite is 6 wt.% at a temperature of 750^{o} C and a depth of 7 km. following a method proposed by Burnham, (1975, 1979) (see Appendix E for calculations). The presence of hydrous phases in some tephras and not in others suggests that

saturation conditions were different at different times.

Estimates of pre-eruptive water contents from this study suggest that 1.5 to 2.75 wt.% H_2O were dissolved in the TVZ rhyolitic magmas which produced TVC and OVC explosive eruptions, while thereoretical studies suggest around 6 wt.%. This discrepency may be resolved with a complete study of delta D systematics for water in TVZ obsidian, or with water determinations in melt inclusions.

CONCLUSIONS

Obsidian inn TVC and OVC tephra is dominantly primary and unaltered. The obsidian partially degassed during the eruptive process prior to quenching, but does contain some portion of pre-eruptive volatiles.

Water and chlorine contents in obsidian show a positive correlation, suggesting that the two volatile species degas at the same rate. An estimate of magmatic water content can be made based on this correlation, along with magmatic values of Cl from glass inclusions in phenocrysts. The pre-eruptive water content is estimated at between 2.5 and 3.75 wt.%, which agrees with values determined for rhyolite magmas by Taylor et. al. (1983).

Temperature and oxygen fugacity buffer trends, determined from co-existing magnetite and ilmenite phenocrysts, demonstrate that different magma types are present in the TVC and OVC. The TVC trends also show that there was a change in TVC magma following the voluminous Oruanui eruption which occured 20,000 yrs. B.P. One tephra, the Taupo plinian, shows anomalously higher temperatures than the others, yielding values of between 900 and 920^{o}C. Glass inclusion geothermometry is consistent with Fe-Ti oxide data, and behavior of the inclusions suggests that they were trapped under high pressure, but this effect has not yet been quantified.

APPENDIX A

Volatiles in magmas

The dominant volatile elements in igneous melts are H, C, F, Cl, and S. H_2O is usually the most abundant molecular volatile species (35-90 mole %), with CO_2 composing 5-50 mole % (Fisher and Schmincke, 1984). Sulfur species are important in mafic magmas, with SO_2 dominant at high temperature and oxygen fugacity, and H_2S otherwise. As the silica content of a melt increases, the S content decreases (Devine et al, 1984). Other volatile species which may be present include H_2, CO, COS, S_2, O_2, HCl, N_2, HF, HB, HI, metal halogens and noble gases. These constituents make up less than 2 mole percent of total volatiles (Fisher and Schmincke, 1984).

Volatiles are defined as "chemical species in gaseous or supercritical fluid state at temperatures over 300-400 C", but this is not necessarily how they occur in magmas (Holloway, 1981). Volatile molecules may be present in a fluid state, but also occur dissolved, or in solution with, the magma (Fisher and Schmincke, 1984). Solution of volatiles can occur with whole molecules or can involve dissociation of molecules to form complexes which can fit into, or bond with, the framework of a silicic magma. The "solubility" of a species refers to the total amount of the component in the melt, regardless of its form. Magmas may contain 20 wt.% dissolved volatiles, although values of 3-5 wt.% are more common in experimental determinations

(Holloway, 1981). This may seem to be a trivial amount, but is actually quite substantial, because although the weight percent is small, the molecular percentage high because volatile elements are very light. For example, if 50% of the molecules in a water-albite melt were H_2O, only 6.4 wt % of the material would be water (Fisher and Schmincke, 1984).

Understanding the solubility mechanism of volatile species in silicate melts is important in order to predict the amount of volatiles which could theoretically be dissolved in the magma. The most common approach is to experimentally study solubilities in a simple system, and then extrapolate the mechanism to a more complex situation.

Solubility of H_2O

The solubility mechanism of water is presently contoversial. Theories for the mechanisms by which water dissolves in a melt have been presented by a number of workers, but no one theory has been agreed upon by all. Several of these theories are outlined in the following paragraphs.

Wasserburg (1957), suggested that water dissolves into a silicate melt by breaking bridging Si-O-Si bonds between tetrahedra and bonding with the open O and Si:

$$Si\text{-}O\text{-}Si + H_2O = Si\text{-}OH\ HO\text{-}Si$$

This model explains the melting point depression of albite seen in a water-albite melt, because the melt becomes depolymerized, resulting in lower albite stability. But, if this is correct, then the molar solubility of H_2O should be proportional to the pressure of water in the system, which is not the case in experimental systems as can be seen in Fig. A-1 (Mysen, 1977). Wasserburg's model is not adequate to describe the behavior of the albite-water system at high water concentrations.

Burnham (1975), proposed a more refined model, which was also based on the water-albite system. It is similar to Wasserburg's, but there are some fundamental differences. The Burnham model was derived from experimentally determined effects of H_2O on the viscosity, electrical conductivity and thermodynamic properties of a water-melt system. It involves the same reaction of H_2O with the bridging Si-O bonds between silica/alumina tetrahedra, but also exchanges a H+ proton with the Na+ which was providing the charge balance on the AlO4 tetrahedra (Fig. A-2) (Burnham, 1979). The reaction of H_2O with Na+ (the left-hand side of Fig. A-2) will go to completion, or will continue up to the point that there is excess H_2O or albite. If the H_2O is greater than 50 mol.% of the melt, the reaction on the right side of Fig. A-2 will begin. The equations for the two reactions are as follows:

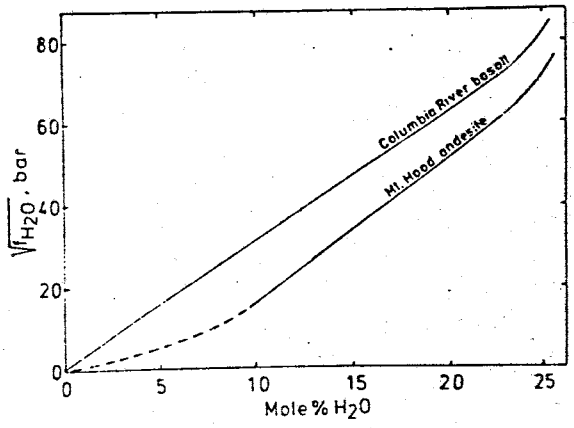

Figure A-1 Molar solubility of H_2O in andesite and tholeiite melt as a function of $(f_{H_2O})^{1/2}$. Solubility data are from *Hamilton et al.* [1964], and fugacity data from *Burnham et al.* [1969].

from Mysen, 1977

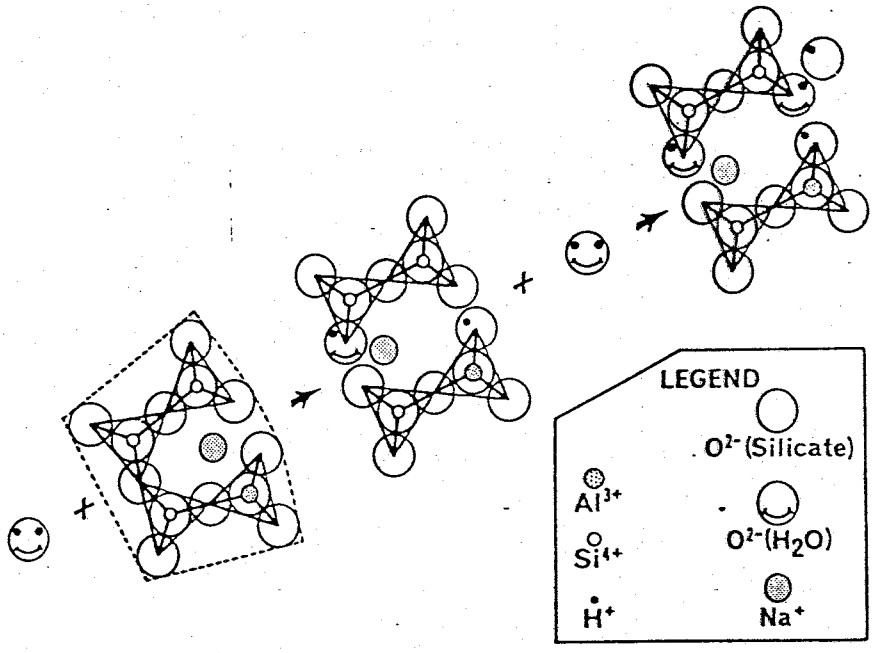

Figure A-2 Proposed reaction scheme for solution of H_2O in $NaAlSi_3O_8$ melts, as expressed in text Eqs. 16-1 and 16-2 (modified from Burnham, 1975a, Fig. 6). The reaction unit (mole) of $NaAlSi_3O_8$ melt represented is as outlined in Fig. 16-1.

from Burnham, 1979

1) $NaAlSi_3O_8 + H_2O = AlSi_3O_8(OH) + NaOH$

2) $AlSi_3O_8(OH) + nH_2O = AlSi_3O_8(OH)$

The second reaction will occur because all of the Na has been used up, so a new mechanism for charge balance must be found. While the first reaction is in progress, one mole of OH- ion associated with the silica tetrahedra is produced. The relationship between the activity of H_2O and the square of its mole fraction in the melt is linear, but once the second reaction begins, this relationship becomes exponential because 2 moles of OH are being produced for every mole of H_2O (Burnham, 1979). The reaction of H_2O with the silicate melt has the effect of depolymerizing the liquid by breaking the tetrahedral bridge bonds and therefore decreasing the stability of polymerized minerals (esp. feldspars). This depolymerization also decreases the density of the melt, which with a mole fraction of 0.5 H_2O can be 10^5 - 10^6 times lower than for an anhydrous melt, allowing crystals to settle more readily (Burnham, 1979). The exchange of H+ for Na+ results in greater mobility of Na+, which should increase the electrical conductivity of the melt. This effect is demonstrated in experimental systems, supporting this model for H_2O solubility. To determine if this model was applicable to more varied igneous systems, Burnham compared experimental solubility data for different composition rocks. Although the actual wt % of dissolved H_2O was different for each sample, the molecular percentage of H_2O was the same, showing that the same

process was taking place in each case (Fig. A-3). Burnham concludes that, as long as each mole of melt contains 1 mole of exchangeable cations, solution of water will behave the same regardless of melt composition.

Infrared spectroscopy (IRS) data on water quenched in natural glasses lead Stolper (1982) to propose another refinement to the water solubility model. He finds that molecular water, as well as OH- ions, are present in quenched glass. Assuming that the speciation of water in glass in representative of that in the melt, he proposes that the reaction: $H_2O + O2 = 2OH$ has equilibrium constants rather than proceeding to completion. The relationship observed between H_2O and OH- groups is summarized in Fig. A-4. At low water contents (< .5 wt%) all water is present as hydroxyl groups, but as water contents become higher, molecular water is seen and becomes more prevalent as water content increases. This seems to fit an equilibrium constant model, with the two components varying inversely. Also, the IRS data demonstrates that water is structurally bound in the glass and does not occur as fluid inclusions, because no ice bands are present at liquid nitrogen temperatures. If the water speciation was different in the glass than in the melt, this theory would be invalid, but the water content and species distribution is independent of quenching history (Stolper, 1982). Stolper's model explains the same phenomena as Burnham's; electrical conductivity, viscosity etc..., but also explains why water solubilities of melts seem to be independent of melt composition

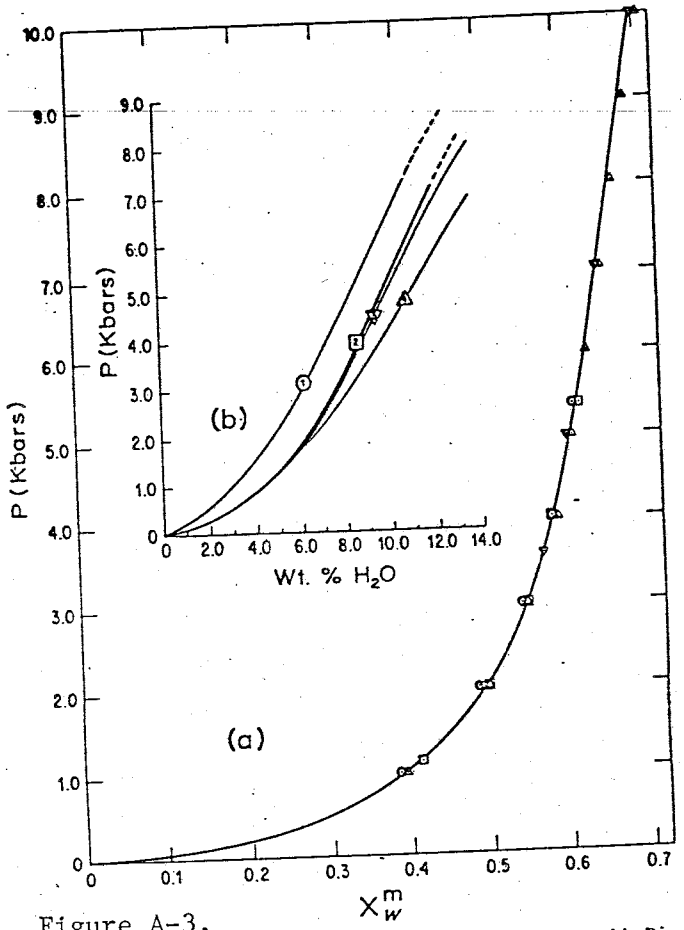

Figure A-3.
Solubility of H_2O in aluminosilicate melts. Circles (1). Columbia River basalt: squares (2). Mt. Hood andesite: inverted triangles (3). albite: and upright triangles (4). Harding pegmatite. (a) Equimolal solubilities at 1373K (1100°C) calculated from experimental weight-percent solubilities in (b). using text Eqs. 16-3, 16-4, 16-5, 16-6, and values of M_e and M_e' from Table 16-1. (b) Experimental weight-percent solubilities at various temperatures. from Burnham and Jahns (1962) and Hamilton *et al.* (1964).

from Burnham, 1979

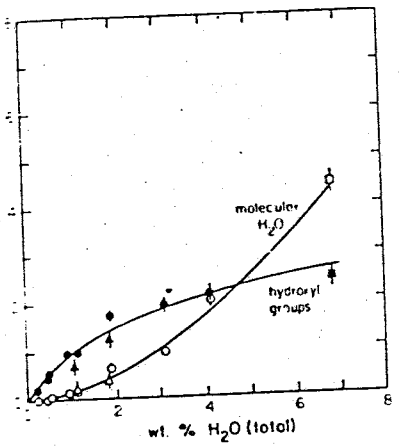

wt % H_2O per species molecular water or hydroxyl groups

Figure A-4. Speciation of H_2O with increasing quantity in the melt.

from Stolper, 1982

at high, but not at low, water contents. The bonding of OH- groups would be compositionally dependent because of the number of tetrahedral bridges available, but structurally bound H_2O groups could enter a melt in the same proportions, regardless of composition (Stolper, 1982). It seems that Burnham's model for OH- configuration is probably correct, but that the effect that Stolper describes would be present at higher H_2O concentrations. Although this problem is not resolved, the effect of dissolved water in silicate melts seems clear, because the polymerization will occur, regardless of the exact solutions process.

Solubility of chlorine

The solubility mechanisms of the other volatile element under consideration, Cl, has not been studied in detail, but Burnham (1979) suggests that it may dissolve by mechanisms similar to that of water:

$$HCl\ (v) + O^{2+}\ (m) = Cl^{-}\ (m) + OH^{-}\ (m)$$

But, because the Cl ion is larger than OH, the solubility would be expected to be lower. Experiments by Kilinc and Burnham (1972) suggest that Cl does strongly partition into a vapor phase, but data from Moore (1970) show that H_2O and Cl in quenched basaltic glasses show a 1:1 correlation, suggesting that they are degassing at the same rate.

Determination of magmatic volatiles

A number of approaches are used to arrive at pre-eruptive volatile contents. They include measuring gases emitted from lava lakes or fumeroles, calculations of volatile fugacities from mineral stabilities or actual measurements of volatiles in glass inclusions or quenched magma.

Sampling of volcanic gases directly from fumeroles or lava lakes is difficult and may not yield accurate data because volatiles have different solubilities, so some may be preferentially retained. Contamination by reaction with meteoric water or atmospheric gases is also a problem. Methods used to overcome these problems involve restoration of true gas contents by complex computer calculations (Gerlach, 1981), but even when this is done, values obtained are purely qualitative, with no quantitative information.

Volatile fugacities in magmas may be determined by the composition and content of phenocrysts in a melt.

Merzbacher and Eggler (1984) have experimentally documented a magmatic geohydrometer based on compositional equilibrium between glass and phenocrysts, generally plagioclase and pyroxene. Presence of varying amounts of water will change the equilibrium of these conponents. From this information, they suggest magmatic water of 4 wt % for the May 18, 1980 eruption of Mount St. Helens.

Another common method of estimating the volatile content of a magma based on the phenocryst assemblage is by thermodynamic calculations. It is not possible to determine the fugacity of all volatiles in the magma from a given phenocryst assemblage, but only ones which are buffered by the phases present.

A simple example of this technique is shown by the calculation of oxygen fugacity from an assemblage including olivine, titanomagnetite, and quartz (Carmicheal, Turner and Verhoogen, 1974):

$$3Fe_2SiO_4 + O_2 = 2Fe_3O_4 + 3SiO_2$$

There is an equilibrium constant K for this reaction at fixed temperature and pressure:

$$K_{P,T} = (a_{Fe3O4})^2(a_{SiO2})^3(a_{Fe2SiO4})^{-3}fo_2^{-1} \quad (1)$$

If all three solid phases are present, then the oxygen fugacity will remain constant for fixed temperature and pressure, because the activity of a solid is always equal to 1. The value of K can be determined thermodynamically:

$$G = G_r + RT\ln K \quad (2)$$

Where G is the change in Gibbs Free Energy of the systen, and G_r is the change in Gibbs Free Energy of reaction (1). R is the gas constant, and T is the temperature. For a system in equilibrium,

G is 0, so:

$$G_r = -RT\ln K \quad (3)$$

By combinding reactions (1) and (3), the following reaction is derived:

$$\log fo_2 = (G_r)(2.303RT)^{-1} + \log[(a_{Fe3O4})^2(a_{SiO2})^3(a_{Fe2SiO4})^{-3} \quad (4)$$

Because the activities of solid phases are 1, fo_2 can be determined, when G_r is known.

The same process can be applied to a number of other volatiles, given the correct mineralogy. For example, sulfur fugacity can be calculated with an assemblage of pyrrhotite, titanomagnetite and olivine (Rutherford and Heming, 1978), hydrogen fugacity with biotite, sanadine and magnetite (Wolff and Storey, 1983), and carbon dioxide with olivine, diopside and magnesian ilmenite (Carmicheal et al, 1974).

The fugacity of water can be determined with an assemblage of cummingtonite, orthopyroxene, and quartz (Ewart et al, 1975). These authors have calculated pre-eruptive water fugacities of tephra from the Taupo Volcanic Zone for samples containing this phenocryst assemblage. They also showed that $P_{H2O} \sim P_{total}$, and calculate pre-eruptive water content between 5.2 and 7.9 wt %. Rutherford and Heming (1978) determined magmatic water contents within about the same range for older TVZ ignimbrites, using a buffer assemblage of biotite, sanidine, and magnetite.

The third method, direct analysis of volatiles in volcanic material can be done by a number of different techniques. The material analysed must be quenched volcanic glass, whether extruded magma or glass inclusions in phenocrysts. Eichelberger et al (1981), analyse water in young rhyolitic obsidians from tephra deposits by thermogravinometric analysis. Their values range from between 0.5 and 3.0 weight percent, decreasing as the eruptions proceed until the final non-explosive flows which contain 0.2 wt % H_2O. These analyses, coupled with deuterium/hydrogen values, which become more negative with increase degassing, show that the original H_2O content of the magmas was close to 3.0 wt % (fig. A-5). This suggests that obsidians can trap all or part of volcanic H_2O.

Volatiles in glass may be analysed by the Penfield method (described by Peck, 1964), and this has been done by Moore (1970), for deep sea basaltic glass. Mass spectrometry has been used to determine ratios of volatiles in Hawaiian volcanic glass, but cannot measure absolute quantities (Muenow, 1973).

The electron microprobe has been used for analyses of glass inclusions, where a beam technique is most easily applied because of the small volume of glass available. Some workers have reported H_2O values based on the "analysis by difference" technique, where the difference of analytical totals from 100% is assumed to be the percentage of H_2O (Anderson, 1973; Sommer, 1977). This is not a very accurate method because it is

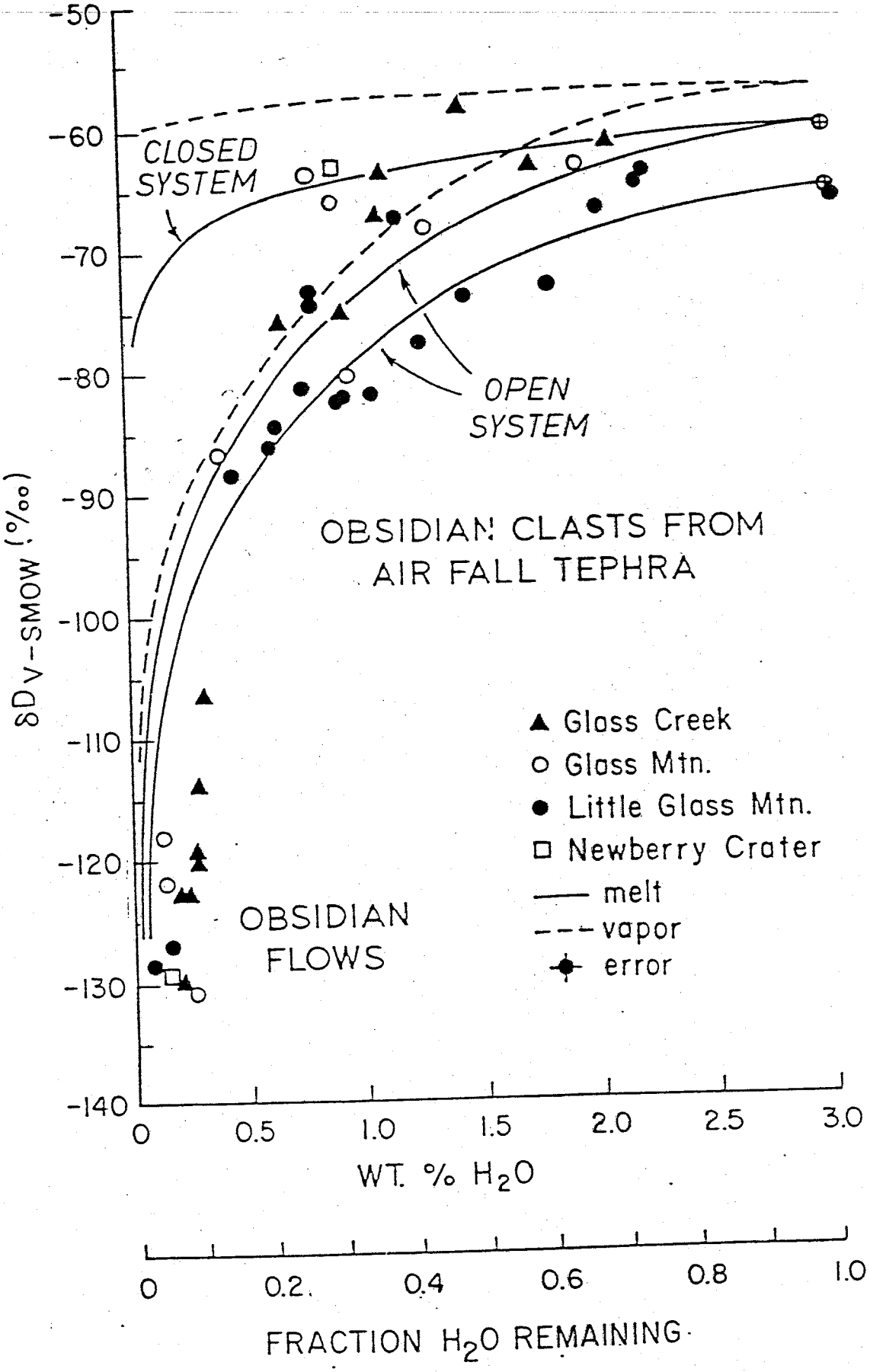

Figure A-5. Delta D versus H_2O, showing fractionation trends.

From Taylor et. al., 1983

impossible to assure that H_2O is accounting for the difference, but it can be used for general approximations. Water cannot be directly determined by microprobe analysis because the X-Rays emitted by H are too low energy to be measured. The microprobe is more applicable for higher Z volatile elements, such as S, Cl, and Fl. The method for these analyses, involving very long count times, is described by Devine et al (1984).

Sommer and Schramm (1983), have devised a method for glass inclusion volatile determinations which requires two major steps: 1) determination of glass concentrations in phenocrysts, and 2) determination of volatile concentrations in glass. The amount of glass is determined by calculating the dilution factor of an element which is present in the glass, but not in the host mineral, and volatiles are measured by partial pressure capacitance manometer. This method, although it involves a lot of work, seems to yield good results. Values they measure for silicic melt inclusions range from 2.11 wt.% to 3.99 wt.% for airfall and from 0.79 wt.% to 1.71 wt.% for associated ash-flow tuff deposits. Analysis of glass inclusions assumes that there are no volatiles included in crystals as dissolved species or as fluid inclusions. This assumption may not be true, but no evidence exists proving if it is valid or not.

APPENDIX B

List of samples from Taupo center.

Number	Unit	Stop	Photo	Type	Comments
83-001	Rotongaio	19	5-6,5-7	B	
83-002	Hatepe phr.	"	"	B	basal 12 cm.
83-003	" "	"	"	B	next 12 cm.
83-004	" "	"	"	B	next 12 cm.
83-005	" "	"	"	B	top 12 cm.
83-006	" "	"	"	B	obs. rich layer 38-40 cm from base.
83-007	Hatepe plin.	"	"	O	
83-008	Motutere	"	"	B	
83-009	Porunui	"	5-9	B	lower 12 cm. of plinian
83-010	Karapiti	"	5-10	B	lower 8 cm.
83-011	" "	"	5-11	B	base of upper 13 cm.
83-012	" "	"	5-10	B	upper 13 cm.
83-013	Rot/Taupo pl.	27	5-14,5-15	B	transition between 2 units
83-014	Taupo pl.	"	"	B	basal 15 cm.
83-015	" "	"	"	B	next 50 cm.
83-016	" "	"	"	O	top of unit (top of sample 15)
83-017	" "	"	"	P	top 20 cm.
83-018	Waihimia	31	5-19,5-20	O	from 1 m. above base
83-019	" "	"	"	P	from 1 to 2 m. above base
83-020	" "	"	"	B	from crystal rich layer
83-021	" "	"	"	P	mixed pumice from 2 m below top
83-022	Taupo pl.	32	5-21,5-22	O	in gulley fill
83-023	Hat. phr.	"	5-23	B	plinian layer 80 cm. up from base of phreatomagmatic
83-024	Marapa	1	4-15	B	basal 15 cm.
83-025	" "	"	"	B	31 cm., 39 cm up from base
83-026	" "	"	"	B	top 10 cm.
83-027	Hatepe pl.	"	"	B	
83-028	Groundlayer	"	"	B	
83-029	Whaikapu	"	"	B	bottom 15 cm., lithic rich
83-030	Opepe	"	"	B	22 cm., 114 cm. up from base
83-031	" "	"	"	B	50 cm., 65 cm. up from base
83-032	" "	"	"	B	basal 65 cm.
83-033	" "	"	"	P	top of unit
83-034	Karapiti	"	"	B	bottom 50 cm.
83-035	" "	"	"	B	top 50 cm.
83-036	" "	"	"	P	top of unit
83-037	Groundlayer	24		O	
83-038	" "	"		O	one large chunk
83-039	Rotengaio	"		B	0-10 cm. from base
83-040	" "	"		B	10-20 cm. from base
83-041	" "	"		B	20-30 cm. from base
83-042	" "	"		B	30-70 cm. from base

83-043	Initial ash	"		B	lower 30 cm.
83-044	Hatepe pl./I.A	"		B	8 cm. between Hat. plin. and Initial Ash
83-045	Hatepe pl.	"		O	
83-046	Hatepe pl.	"		P	
83-047	Okaia	10	4-28	B	top 85 cm.
83-048	Okaia	"	"	B	basal 20 cm.
83-049	Oruanui	"	"	B	layer 1, 20 cm.
83-050	" "	"	"	B	layer 2, 4 cm.
83-051	" "	9		B	layer 3
83-052	" "	"		B	basal airfall
83-053	" "	10	4-28	B	layer 1, 22 cm.
83-054	Tihoi	"	"	B	top 57 cm.
83-055	" "	"	4-28	B	top 40 cm.
83-056	Okaia	33-b		B	
DOBS	Ben Lomond Obs.	4	4-22	O	obsidian flow

B = bulk sample
P = pumice picked at outcrop
O = obsidian picked at outcrop

List of samples from Okataina center.

Number	Unit	Stop	Photo	Type	Comments
83-057	Terere	35	6-6	B	basal 10 cm.
83-058	" "	"	"	B	next 11 cm.
83-059	" "	"	"	B	next 10 cm.
83-060	" "	"	"	B	top 15 cm.
83-061	------	36			glassy skin of lava flow
83-062	Rotoma	37	6-7	B	coarse layer 30-70 cm from base
83-063	" "	"	"	B	next 60 cm.
83-064	" "	"	"	B	top 140 cm.
83-065	Mamaku	38	6-8,6-9	B	55-65 cm. from base
83-066	" "	"	"	B	165-175 cm. from base
83-067	" "	"	"	B	30 cm. layer above 1st ign.
83-068	Whakatani	39	6-10	B	fine layer 3m. above base
83-069	" "	"	6-11	P	pumice from base
83-070	Mangaone	40	6-12	B	basal 39 cm.
83-071	" "	"	"	B	next 24 cm.
83-072	Awakeri	"	6-13	B	
83-073	Omateroa	41		P,O	1 m. above base
83-074	" "	"		O	4.5 m. above base
83-075	" "	"		O	2 m. above base
83-076	Okareka	42	6-15	B	60-100 cm. up from base
83-077	" "	"	"	P	16-43 cm. up from base
83-078	Rerewhai.	43	6-16	B	0-38 cm. from base
83-079	" "	"	"	B	42 -65 cm. from base
83-080	Kaharoa	44	6-17	B	60 cm. up from base
83-081	Waiohau	45	6-18	B	Obs. rich layer 40 cm. up from base
83-082	Oruanui	46	6-20	B	unit 1
83-083	Rotarua	34	6-22,23,24	O	coarse bed 1.5 m. from base
83-084	" "	"	"	P	coarse bed 1.5 m. from base
83-085	" "	"	"	B	1 m. above base
83-086	" "	"	"	O	base
83-087	" "	"	"	O	1 m. above base
83-088	" "	"	"	O	2.5 m. above base
83-090	" "	"	"	P	2.5 m. above base
83-091	" "	"	"	B	2.5 m. above base

B = bulk sample
P = pumice picked from outcrop
O = obsidian picked from outcrop

APPENDIX C

List of Sample Localities

Location of sample localities listed in Appendix B.

Locality number	Location
1	DeBretts Section. Highway 5, 0.25 km. west of junction with Crown Rd. NZMS 1 N94/579353
4	Poihipi Rd., 2.5 km. southwest of junction with Whangamata forestry Rd. NZMS 1 N93/435050
9	Whangamata Rd., 2 km. southwest of junction with Waihora Rd. NZMS 1 N93/312456
10	Whangamata Rd. 0.5 km. southeast of junction with Otake Rd. NZMS 1 N93/374457
19	Mission Bay Rd. NZMS 1 N103/491076
24	Unnamed forest rd. 1.5 km southeast of Highway 1. NZMS 1 N103/493158
27	Highway 5, 0.75 km. northwest of Opepe monument NZMS 1 N103/680280
31	High Level Rd., 2 km. southwest of junction with Mere Rd. NZMS 1 N103/689190
32	High Level Rd., 3.5 km. southwest of junction with Mere Rd. NZMS 1 N103/677184
34	Quarry on Tawarewa-Okareka loop Rd. NZMS 152 793002
35	Highway 30 at Huaparu Bay. NZMS 152 877148
36	Unnamed forest rd., 1.5 km. south of Highway 30.

	NZMS 152 915130
37	Unnamed forest rd., 4 km. south of Highway 30. NZMS 152 925110
38	NZMS 1 N77/919105
39	NZMS 1 N77/956075
40	NZMS 1 N77/181093
41	NZMS 1 N77/184015
42	NZMS 1 N77/131943
43	NZMS 1 N86/995825
44	NZMS 1 N86/971868
45	NZMS 1 N85/897820
46	NZMS 1 N85/726661

Kilometer distances are estimates.

Appendix D

Part 1- Water Analyses

Dupont Moisture Analyser

Water in obsidian fragments was analysed with a Dupont Moisture Analyser at Sandia National Laboratories, N.M. This method involves heating ground obsidian to a point where all structurally bound water is released. This water is carried by He gas to a P_2O_5 cell across which electrical potential is applied. The water is absorbed by the cell, causing it to become conductive and the water becomes electrolysed. The current required to electrolyse water in the entire sample is proportional to the amount of water which the sample contained. The weight percent water can be calculated from the exact weight of the sample and calibration factors.

Procedure

1) Grind obsidian fragments to 75 mesh with an agate mortar and pestle, using acetone as a grinding medium.

2) Dry in a 100^{o} C oven overnight. Store in dried vials. Redry in a vacuum oven at 100^{o} C vacuum oven for an hour prior to analysis.

of this degree would not seriously affect the results.

Table D-1-1. Multiple analyses of samples on Dupont Moisture Analyser, under same conditions.

sample	results (wt.% H_2O) run 1	run 2	run 3	mean	standard deviation	percent variance
83-008	1.60	1.56		1.58	0.020	1.0
83-076	0.91	0.94		0.93	0.015	1.6
83-009	1.01	0.82		0.92	0.095	10.2
DOBS	0.29	0.29	0.27	0.28	0.009	3.2

3) Load approximatly 100 mg. (weigh exactly) into a platinum boat and place in furnace.

4) Heat to 900° C for 20 minutes. Water is constantly transfered to the P_2O_5 cell and counts accumulate.

5) After 20 min., remove sample and note counts.

Before running samples, a blank capillary and two capillaries containing 2 mg. of water were analysed. Subsequently, 2 capillaries also containing 2 mg. of water were analysed after a set of six unknowns were run. The resulting calibration is of the following form:

$$\text{wt.\% } H_2O_{sam.} = (\text{sam. cts.} - \text{bkg. cts.}/\text{ sam. wt.}) \times K$$

$$K = (\text{cap. } H_2O \times 100)/(\text{cap. cts.} - \text{bkg. cts.})$$

All weight measurements in this equation are in milligrams.

Analytical precision and accuracy of this technique were found to be <1% and <5% respectivly by Eichelberger and Westrich (1981). In order to test this, several samples were run in duplicate or triplicate. The results can be seem in Table D-1-1.

One of the percent of variance values is quite high (10%), but the others are good. The high value seems to be the exception rather than the rule, but even an occaisonal variance

Karl Fisher Titration

The second method used for water analyses was Karl Fisher titrometry. This technique involves titrating the unknown quantity of water in a pyridine-mehtanol solution containing iodine ion (I^-) and SO_2 as principle components. The following reaction occurs: $I_2 + SO_2 + H_2O = 2HI + SO_2$ (1)

As reaction 1 proceeds, iodine ion is generated by electrolysis at the anion. The H_2O/I_2 reaction always occurs in 1:1 proportions, so the amounts on H_2O introduced to the solution (H_2O content of the sample) is directly proportional to the amount of electricity necessary to regenerate the I_2.

The sensivity of this technique has been evaluated by the manufacturer at 0.1 micrograms of H_2O, and the precision is + 3 micrograms for a sample size of between 10 micrograms and 1 mg. of H_2O. Although this may be true under ideal conditions for perfectly homogenous samples, precision of the analyses done so far have not been this good. Initial results suggest that precision is often this good for sample containing several hundred micrograms of H_2O, but that multiple runs of some samples do not fall within these limits, probably due to sample inhomogeniety. Samples run on different days, tend to show worse precision, probably due to different drying conditions, or differences in atmospheric humidity. Work evaluating precision of the technique is still in progress.

The same basic technique is used to extract the water from the obsidian as for the Dupont Moisture Analyser, although there are a few differences. The method is as follows:

1) Prepare sample, either by grinding or by cleaning obsidian fragments in an ultrasonic bath.

2) Dry overnight at 100^{o} C.

3) Load sample into a sample boat. A wide range of weights are acceptable, but it is best to use more than 10 mg.

4) Place sample in furnace, and heat to 100^{o} C for approximately 2 mins, to drive off any H_2O adsorbed during weighing. Then heat to 950^{o} C for 10-15 mins., and begin titrating at 250^{o} C. Heating may be required for longer than 15 minutes if titration is still continuing at that point.

The main advantage of this technique over the Dupont Moisture Analyser is that the accuracy is good at low quantities of H_2O, so it is possible to analyse individual obsidian fragments. Other advantages are that each analysis takes slightly less time, and because the technique is direct, not relative, there is no need for standardization. Analyses from the Karl Fisher titration method compare favorably with those from the Dupont Moisture Analyser, although the drying process in the furnace usually reduces values by 0.1 wt. % H_2O. Values for samples run by both methods are shown in Table D-1-2.

Table D-1-2. Comparason of water values from the Dupont Moisture Analyser (DMA) and Karl Fisher Titration (KFT).

Sample	H_2O by KFT (wt. %)	H_2O by DMA (wt. %)	% variance about mean
002	0.46	0.42	4.5
003	0.58	0.56	1.8
004	1.56	1.55	0.3
005	1.12	1.07	2.3
006	1.26	1.59	11.6
014	0.45	0.43	2.3
015	0.23	0.24	2.1
016	0.52	0.49	2.9
026	0.90	1.20	14.2
030	1.00	1.16	7.4
031	1.02	1.41	16.0
032	1.10	1.44	13.4
057	0.73	0.78	3.3
059	0.54	0.60	5.3
070	1.49	1.52	1.0
071	1.48	1.68	6.6
DOBS	0.29	0.10	48.7

Part 2- Chlorine Analyses

Chlorine in glass inclusions and obsidian is analysed by a technique similar to that described by Devine et al (1984). The chemical analyses were obtained using a JEOL-733 superprobe at Victoria University, N.Z., with the following operating conditions: 15kv accelerating voltage, 2.5×10^{-8} amp beam current and a beam broadened to 20 microns to reduce volatilization. The Cl analyses each involved a peak search and then three 50 second counts on the peak and one 75 second count on each background.

Normal analytical methods cannot be used for elements such as Cl, S, and F because the very low concentrations require such long counting times. Therefore, the full suite of major elements are not analysed and usual calibration techniques are not possible. Instead, the element is initially calibrated to the microprobe's internal standard, but, in addition, two standards of similar chemical composition as Taupo rhyolites are analysed as unknowns, and a second calibration factor is calculated. This factor is then applied to the analytical results in order to determine true values.

Table D-2-1 shows accepted Cl values for standards KN-18 and KE-12, along with mean analytical results, standard deviation and percent variance.

Table D-2-1. Accepted and analytical values for Cl standards.

standard	accepted Cl value (wt. %)	mean deter. (wt. %)	st. dev.	% variance
KN-18	.37	.257	.017	6.9
KE-12	.33	.248	.014	5.7

The best fit line for these points has the equation:

$y = 1.4x$

So, in order to determine true Cl content from the analytical data, the calibration factor is 1.4.

analysed Cl value x 1.4 = true Cl value

Although this analytical method is not very sophisticated, it seems applicable to elements such as Cl, S, and F, which are not normally analysed by electron microprobe. The lack of matrix correction could be a problem, but the standards used to determine the calibration factor have similar chemistry to the TVZ samples.

The detection limits for Cl by this method are 0.016 wt.% or 160 ppm., and for SO_3 is 0.048 or approximatly 200 ppm S. Sulfur in all Taupo samples was below this detection limit, so calibration data is not included in this paper.

Part 3: Magnetite/ilmenite geothermometry

The composition of magnetite and ilmenite from Taupo and Okataina tephras were determined by electron microprobe analysis.

Polished thin sections were prepared from crystals sorted with a hand magnet, and polishing was done using only diamond grit, so as not to introduce any contaminants. Grains containing both magnetite and ilmenite were found using a reflected light microscope with crossed polarizers, where magnetite remains extinct and ilmenite shows pleiochroic behavior, changing from light to dark with every 90 degrees of rotation. Grains containing both species were photographed and circled with a thin ink line for easy location during analysis. Slides were then carbon coated.

Microprobe analyses were made using an ARL microprobe at the University of New Mexico. Operating conditions were: 15 Kev; 20 nanoamps; average beam current, 1.2×10^{-8} amps; beam size, approximatly 1 micron; and count times of 10 seconds. The Bence-Albee method of raw data correction was used, with known standards of magnetite and ilmenite. These standards were also used as checks to ensure that the calibration was maintained. Three or four grains were analysed per sample, and 2 to 6 points of magnetite and ilmenite each were analysed per grain, as many as possible on different magnetite and ilmenite blebs. Chemical analyses of magnetite and ilmenite done by electron microprobe

are shown in Table D-3-1.

Once the data had been accumulated, temperature and oxygen fugacity were calculated based on the method established by Buddington and Lindsley (1964), using a computer program written by Stormer (1983). The program initially converts total iron determined by the microprobe into divalent and trivalent species, both for magnetite and ilmenite, then calculates temperature and oxygen fugacity by methods proposed by Stormer (1983); Carmichael (1967); Anderson (1968); and Lindsley and Spencer (1982). Values from the Stormer method were used in this paper for reasons explained by Stormer (1983).

Table D-3-1. Magnetite and ilmenite analyses from the Taupo and Okatiana Centers, done by electron microprobe. Each grain (A,B,C,D) represents a number (n) of analyses of magnetite and ilmenite inclusions in one silicate phenocryst.

Taupo Center

Unit	grain	type of crystal	n	oxide wt.% Ti	Fe	Mg
Taupo plinian (017)	A	mag.	3	13.7	78.1	1.0
	B	mag.	3	13.2	78.7	1.0
	C	mag.	3	13.8	79.2	1.0
	A	ilm.	3	45.7	47.1	2.0
	B	ilm.	4	44.5	47.6	1.8
	C	ilm.	4	45.0	47.3	1.8
Hatepe plinian (027)	A	mag.	4	13.5	78.2	1.2
	B	mag.	6	13.7	77.8	0.9
	C	mag.	5	13.1	77.4	0.9
	A	ilm.	11	47.3	46.9	2.0
	B	ilm.	2	47.4	46.6	1.8
	C	ilm.	5	47.6	47.1	2.1
Initial ash (044)	A	mag.	4	12.3	76.6	1.0
	B	mag.	4	11.6	76.8	0.9
	C	mag.	4	11.5	76.3	0.9
	A	ilm.	3	47.8	47.4	1.9
	B	ilm.	3	47.7	47.6	1.8
	C	ilm.	4	46.5	47.3	1.8
Marapa (025)	A	mag.	3	12.7	78.1	1.0
	B	mag.	3	12.7	77.3	0.9
	A	ilm.	2	47.4	47.5	1.5
	B	ilm.	2	46.9	46.6	1.9
Waikapu (029)	A	mag	4	13.9	79.8	0.8
	B	mag.	3	14.3	79.5	0.7
	A	ilm.	2	46.5	46.4	1.2
	B	ilm.	2	46.1	46.3	1.3
Waihimia (020)	A	mag.	3	13.6	76.0	0.8
	C	mag.	2	13.8	76.1	0.7
	A	ilm.	6	47.65	47.0	1.5
	C	ilm.	2	47.9	47.4	1.6
Motutere (008)	A	mag.	3	12.9	80.1	0.8
	B	mag.	4	13.0	77.7	0.8
	C	mag.	2	12.9	77.6	0.8

	D	mag.	2	13.4	77.8	0.7
	A	ilm.	3	47.8	46.9	1.4
	B	ilm.	2	46.6	46.7	1.8
	C	ilm.	2	46.9	46.4	1.6
	D	ilm.	3	46.7	47.0	1.5
Opepe	A	mag.	2	13.7	79.3	0.8
(031)	B	mag.	4	13.0	78.5	0.8
	C	mag.	2	12.3	77.5	0.8
	D	mag.	2	13.0	77.8	0.8
	A	ilm.	3	46.6	46.7	1.6
	B	ilm.	3	45.5	46.9	1.5
	C	ilm.	1	45.9	46.1	1.5
	D	ilm.	2	45.5	46.2	1.5
Porunui	A	mag.	2	13.0	78.9	0.6
(009)	B	mag.	3	13.7	77.5	0.7
	C	mag.	3	13.6	78.3	0.7
	D	mag.	3	13.6	78.6	0.7
	A	ilm.	2	45.5	47.7	1.3
	B	ilm.	2	46.2	46.4	1.3
	C	ilm.	3	47.9	47.0	1.5
	D	ilm.	6	45.1	46.9	1.3
Karapiti	A	mag.	3	13.6	78.0	0.6
(010)	B	mag.	3	13.6	75.9	0.8
	C	mag.	3	13.7	76.3	0.5
	A	ilm.	1	40.8	41.1	1.4
	B	ilm.	4	45.0	45.1	1.3
	C	ilm.	5	45.5	45.8	1.3
Oruanui	A	mag.	5	10.2	81.0	0.5
(050)	B	mag.	3	9.2	82.7	0.6
	C	mag.	4	8.5	83.0	0.8
	D	mag.	4	11.0	82.2	0.6
	A	ilm.	3	47.2	47.6	1.3
	B	ilm.	3	47.1	48.3	1.6
	C	ilm.	4	46.3	47.9	1.7
	D	ilm.	5	47.4	48.4	1.6
Okaia	A	mag.	3	9.3	80.9	0.5
(047)	B	mag.	4	9.3	79.5	0.7
	C	mag.	2	8.6	78.7	0.6
	A	ilm.	5	45.5	45.9	1.3
	B	ilm.	5	44.5	45.8	1.5
	C	ilm.	6	43.4	45.5	1.9
Tihoi	A	mag.	6	9.9	80.0	0.5
(054)	C	mag.	6	8.2	79.9	0.6
	A	ilm.	3	46.1	46.6	1.6
	C	ilm.	4	44.9	45.5	1.1

Okataina Center

Kaharoa	A	mag.	3	8.9	81.8	0.3
(080)	B	mag.	3	8.4	79.2	0.9
	A	ilm.	4	44.7	49.4	1.0
	B	ilm.	3	45.9	44.5	1.9
Whakatani	A	mag.	3	8.1	82.4	0.6
(068)	B	mag.	3	7.7	81.9	0.7
	C	mag.	4	8.0	82.5	0.6
	D	mag.	3	8.6	80.2	0.7
	A	ilm.	3	45.8	47.2	1.4
	B	ilm.	3	44.7	47.3	1.5
	C	ilm.	2	46.5	47.2	1.7
	D	ilm.	4	44.4	46.7	1.5
Mamaku	A	mag.	3	7.5	82.7	0.6
(066)	B	mag.	2	8.3	81.8	0.7
	C	mag.	4	8.3	82.5	0.6
	D	mag.	2	7.4	77.1	0.7
	A	ilm.	2	46.8	47.6	1.6
	B	ilm.	2	46.3	47.4	1.6
	C	ilm.	3	45.8	47.3	1.9
	D	ilm.	1	43.1	46.9	1.7
Rotoma	A	mag.	2	4.6	84.0	0.7
(064)	B	mag.	2	7.2	80.8	0.7
	C	mag.	3	7.2	81.8	0.7
	D	mag.	4	7.6	81.4	0.7
	A	ilm.	2	43.9	48.6	1.7
	B	ilm.	3	44.8	47.7	1.6
	C	ilm.	3	43.5	47.7	1.7
	D	ilm.	2	44.0	47.9	1.7
Waiohau	A	mag.	3	7.8	91.3	0.7
(081)	B	mag.	2	7.5	92.3	0.8
	C	mag.	2	7.5	90.7	0.8
	A	ilm.	2	45.6	47.8	1.7
	B	ilm.	2	45.2	48.7	1.7
	C	ilm.	4	45.3	48.5	1.8
Rotorua	A	mag.	2	8.3	82.4	1.2
(085)	B	mag.	3	8.3	82.2	1.1
	C	mag.	2	8.0	82.5	1.0
	A	ilm.	3	43.1	50.4	2.2
	B	ilm.	4	43.8	50.3	2.2
	C	ilm.	2	43.3	50.0	2.2
Terere	A	mag.	3	7.5	74.9	0.9
(059)	B	mag.	5	7.9	82.3	1.1
	C	mag.	4	7.9	82.5	0.8
	A	ilm.	2	42.3	46.8	1.9

	B	ilm.	4	43.8	47.3	2.0
	C	ilm.	2	43.4	46.5	1.9
Awakeri	A	mag.	3	8.4	80.5	0.9
(072)	B	mag.	3	8.4	80.5	0.9
	C	mag.	3	8.4	80.3	0.9
	A	ilm.	4	46.0	48.1	2.1
	B	ilm.	3	45.8	48.1	1.9
	C	ilm.	4	45.2	47.8	2.0
Mangaone	A	mag.	2	7.7	92.4	1.0
(071)	B	mag.	2	8.2	91.6	1.0
	C	mag.	3	8.2	92.4	1.0
	A	ilm.	3	44.2	48.7	2.1
	B	ilm.	3	44.7	48.5	2.1
	C	ilm.	2	44.1	49.1	2.0

mag. = magnetite
ilm. = ilmenite

Part 4: Glass Inclusion analyses

The basic technique used to determine melt and homogenization temperatures of glass inclusions was to heat the inclusion on a carefully controlled microscope heating stage. During heating, observe the behavior of the inclusion, noting changes in the inclusion's appearance, and the temperatures at which they occur.

The crystals containing inclusions used for analyses were doubly polished in order to assure good visibility of the inclusions, especially at high temperatures when optics become distorted. The thickness of the chip is not very important for transparent minerals such as quartz and feldspar, in fact, thicker chips are often desirable because more inclusions will be present in a given chip.

The stage used for heating measurements is a Linkham 1500, calibrated using standards shown in Table D-4-1:

Compound	True Melt Temp. (C)	Indicated Melt Temp. (C)
$NaNO_3$	307	420
$K_2Cr_2O_7$	398	550
AgI	558	748
KI	683	932
KCl	776	1048
NaCl	801	1093
Cu	1083	topped out at 1385

From this, a calibration curve was prepared, shown in Fig. D-4-1. Once calibrated, the stage remained quite stable, although the maximum attainable temperature constantly dropped due to corrosion problems with the connection between the power supply and the heating element. Before running samples, a bracketing high and low standard were run to ensure that the calibration had been maintained.

The sample was heated quickly (~100^{o}C/min) to the melting point. Once melting was attained, heating proceeded more slowly, leaving samples at higher temperatures for 5 to 30 minutes, because homogenization requires dissolution of gas into melt and kinetics of melt/gas reactions are slow. Because so few inclusions were analysed, no standard post-melting procedure has yet been established.

The melting point in these silicate inclusions from the Taupo Volcanic Zone are often not easy to pinpoint, because the appearance of the inclusion does not change much. Some changes which occur, indicating melting, include: subtle movement of the vapor bubble, simultaneous nucleation of a number of small bubbles, change in vapor bubble size, or color change of the glass. All of these criteria, except color change, are definite indications that the glass is melted, but show maximum melt temperature, because the glass may be molten for some time before any of these changes occur.

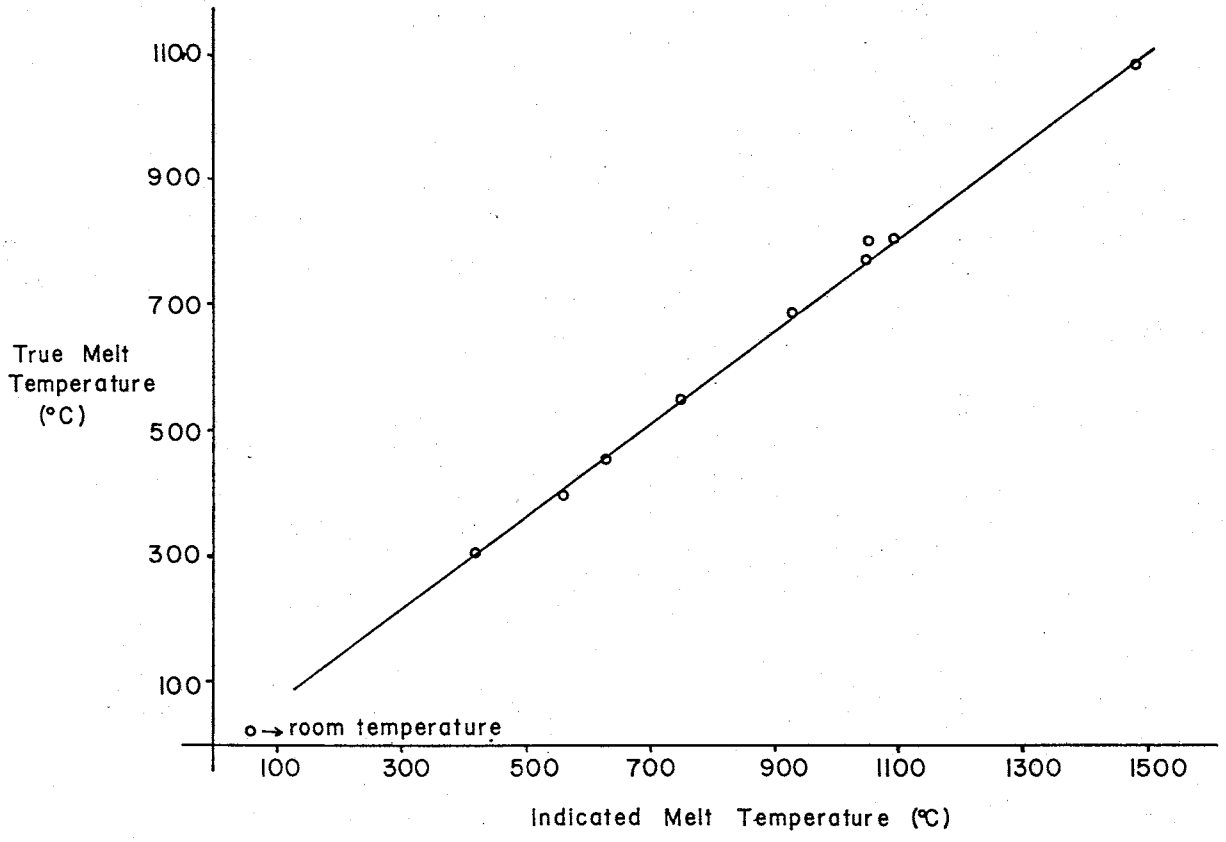
1100
900
700
500
300
100
True Melt Temperature (°C)
o → room temperature
100
300
500
700
900
1100
1300
1500
Indicated Melt Temperature (°C)

The information given from glass inclusion analyses is interesting, but will require more extensive work before it is really understood.

Appendix E

Calculated solubility for Taupo Volcanic Rhyolites

Burnham (1975, 1979) devised a model for solubility of H_2O in magmas which allows theoretical solubilities to be calculated for any given magma as long as the chemical composition is known. This model explains that H_2O dissolves in melts by breaking Si-O-Si bridges, and bonding with the available oxygen. If cations are present, balancing the charge on Al tetrahedra, they will move to occupy a position near the broken bridge site to maintain electrical neutrality. The reaction is the following, and will occur for up to 50 mole % H_2O in a pure albite melt. Terms used in all of the following equations are defined in Table E-1.

$$H_2O_{(v)} + O^{2-}_{(m)} + Na^+ = OH^-_{(m)} + ONa^-_{(m)} + H^+_{(m)} \qquad \text{Eq. 1}$$

If no cations are available, H_2O will dissolve according to the following reaction, producing 2 moles of OH^- for every mole of dissolved H_2O. This reaction will take place if more than 50 mole % H_2O is present in the melt.

$$H_2O_{(v)} + O^{2-}_{(m)} = 2OH^-_{(m)} \qquad \text{Eq. 2}$$

Table E-1 . Definition of equation variables, in order of occurence in the text.

v : vapor phase

m : melt phase

M_e : equivalent mass of melt relative to H_2O

n_i^x : moles of exchangeable cations

n_{Si} : moles of silica

a_w : activity of water in the melt

k : constant (must be calculated for each case)

x_w^m : mole % of H_2O in melt

T : temperature in degrees Kelvin

W_w^m : weight % H_2 in melt

M_e' : equivalent mass of melt relative to H_2O for greater than 50 molecular percent

W_w^m : weight fraction of H_2O in melt in excess of 50 molecular percent

Table E-2. Calculation of equivalent weights of Taupo Volcanic Zone Rhyolite to albite. Average analysis of rhyolite from Reid (1983)

element	weight %	mole % cation	mole % oxygen
SiO_2	73.7	1.23	2.46
TiO_2	0.29	0.004	0.008
Al_2O_3	13.3	0.261	0.391
Fe_2O_3	1.82	0.023	0.034
MgO	0.36	0.009	0.009
CaO	1.67	0.030	0.030
Na_2O	4.28	0.138	0.069
K_2O	3.17	0.067	0.034
total	98.62	1.762	3.056

Equivalent mass: $98.62\ [1\ /(0.267 + 0.19\{1.23 - (3 \times 0.267)\})] = 283$
(less than 50 mole % H_2O)

Equivalent mass: $98.62\ (8/3.056) = 258$
(greater than 50 mole % H_2O)

Burnham's solubility model is for a pure albite melt, but he has found that it can be applied to any magma by calculating the mass of rock melt which will interact with one mole of H_2O. Calculation of this mass is different for amounts of water greater or less than 50 mole %, because of the different solubility mechanisms operating at the different water contents. When the water content is more than 50 mole %, the reaction is simple (eq. 2), and is proportional to the molecular percentage of oxygen, as long as there was not more than 1 mole of exchangeable cations present in the original melt.

If less than 1 mole of water is present, the reaction is more complex because of the interaction of exchangeable cations. The exchangeable cations are proportional to the amount of Al in tetrahedral co-ordination, so in a melt with no normative corundum, the number of moles of melt which will react with water is proportional to the moles of Al. When there is normative corundum, the process is more complex, and the amount of melt which will react with water is shown by the equation:

$$M_e = 1/[\ n_i^x + 0.19(n_{Si} - 3\ n_i^x)] \qquad \text{Eq. 3}$$

The masses of one mole of rock melt, in terms of interaction with water, are calculated for an average Taupo Volcanic Zone rhyolite (Table E-2).

Burnham (1975) showed that there is a linear relationship between the activity and molecular percentages of water for less than 50 mole % H_2O in the melt:

$$a_w = k(x_w^m)^2 \qquad \text{Eq. 4}$$

When there is more than 50 mole % H_2O, the relationship changes from linear to exponential because 2 moles of OH^- are produced for each mole of H_2O in solution:

$$a_w = 0.25ke^{(6.52 - 2667/T)(x - 0.5)} \qquad \text{Eq. 5}$$

Based on these equations, a solubility curve can be calculated for an albite melt at 750° C, using values for k from chart 16-3 (Burnham, 1979). The maximum solubility is shown by setting the activity of water equal to 1, and assuming that a very small amount of vapor is present. Values graphed in Fig. E-1 and listed in Table E-3.

Once this solubility curve is determined, the weight percent of H_2O at a range of pressures can be calculated for Taupo rhyolite at 750° C by using the following two equations:

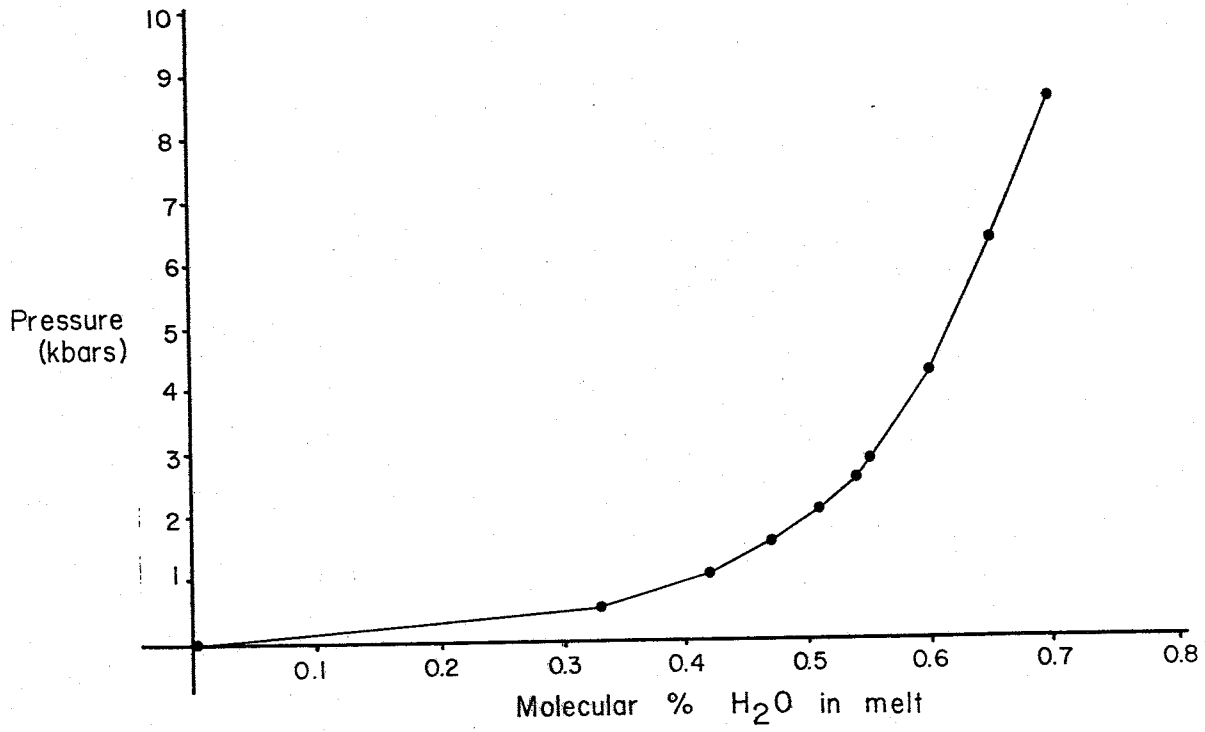

Figure E-1. Maximum solubility of H_2O in an albite melt at 750°C.

Table E-3. Maximum solubility of water in an albite melt at 750° C, from equations 4 and 5 in text. Values for k are from Fig. 16-3 (Burnham, 1979).

Pressure (kb)	ln k	molecular % H_2O (x_w^m)
0.001	8.25	0.016
0.05	2.2	0.33
1	1.75	0.42
1.5	1.51	0.47
1.95	1.39	0.5
2	1.35	0.51
2.5	1.25	0.54
3	1.19	0.55
4.2	0.99	0.60
6.3	0.80	0.65
8.5	0.60	0.70
18	0.20	0.80

For less than 50 mole % H2O:

$$x_w^m/(1 - x_w^m) = (M_e W_w^m)/[18.02(1 - W_w^m)] \qquad \text{Eq. 6}$$

For greater than 50 mole % H2O:

$$x_w^m/(1 - x_w^m) = 1 + [(M_e' \ W_w^m)/\{18.02(1 - \ W_w^m)\}] \qquad \text{Eq. 7}$$

Values calculated for the TVZ rhyolite are shown in Fig E-2, and are listed in Table E-4.

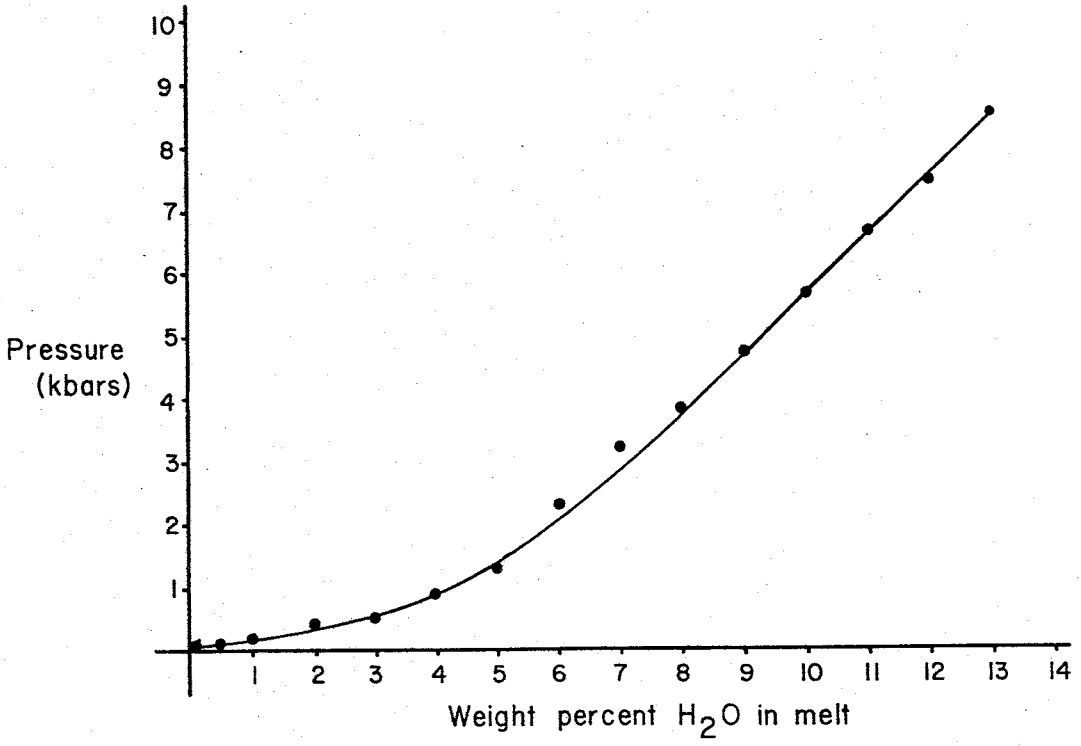

Figure E-2. Maximum solubility of water in an average TVZ rhyolite at 750°C.

Table E-4. Molecular and weight percent H_2O which would be soluble in an average Taupo Volcanic Zone rhyolite (750°C), for different temperatures. For any given weight percent H_2O (W_w^m), the molecular percent H_2O is calculated from equations 6 and 7 in the text. Pressure at a determined molecular percentage of water is read from Fig. E-1(text).

Weight fraction H_2O (W_w^m)	Molecular fraction H_2O (x_w^m)	Pressure (kbars)
0.001	0.02	~0.001
0.005	0.04	0.05
0.01	0.14	0.2
0.02	0.24	0.4
0.03	0.33	0.5
0.04	0.40	0.9
0.05	0.45	1.3
0.06	0.53	2.3
0.07	0.56	3.2
0.08	0.59	3.8
0.09	0.62	4.7
0.10	0.64	5.6
0.11	0.66	6.6
0.12	0.68	7.4
0.13	0.69	8.5

References Cited

Anderson, A.T., 1968. Oxidation of the LaBlanche Lake titaniferous magnetite deposit, Quebec. J. of Geol., 76, 528-47.

Anderson, A.T., 1973. The before-eruption water content of some high alumina magmas. Bull. Volcan., 37, 530-52.

Beddoe-Stephens, B., Aspden, J.A. and Shepherd, T.J., 1983. Glass inclusions and melt compositions of the Toba Tuffs, Northern Sumatra. Contrib. Mineral. and Petrol., 83, 278-87.

Blattner, P., and Reid, F.W., 1982. The origin of lavas and ignimbrites of the Taupo Volcanic Zone, New Zealand, in light of oxygen isotope data. Geochim. Cosmochim. Acta, 46, 1417-29

Buddington, A.F., and Lindsley, D.H., 1964. Iron-titanium oxide minerals and synthetic equivalents. J. Petrol., 5, 310-57.

Burnham, C.W., 1979. Importance of volatile constituents. In Yoder, H.S. Ed, Evolution of igneous rocks, 50 anniversary perspectives. Princeton Univ. Press, Princeton, N.J., 439-82.

Burnham, C.W., 1975. Water and magma; a mixing model. Geochim. Cosmochim. Acta, 39, 1077-84.

Carmicheal, I.S.E., 1967. The iron-titanium oxides of salic volcanic rocks and their associated ferromagnesian silicates. Contrib. Mineral. Petrol., 14, 36-64.

Carmicheal, I.S.E., Turner, F.J., and Verhoogen, J., 1974. Igneous Petrology. McGraw-Hill Book Co., New York.

Cole, J.W., 1979. Structure, petrology, and genesis of cenozoic volcanism, Taupo Volcanic Zone, New Zealand--a review. New Zealand J. Geol. Geophys., 22, 63-

----------, 1984. Taupo-Rotarua Depression: an ensialic marginal basin of North Island, New Zealand. In: Marginal Basin Geology, eds: B.P. Kokelaar and M.F. Howells. Blackwell Scientific Publications.

Devine, J.D., Sigurdsson, H. and Davis, A.N., 1984. Estimates of sulfur and chlorine yield to the atmosphere from volcanic eruptions and potential climatic effects. J. Geophys. Res., 89, 6309-25.

Eichelberger, J.C. and Westrich, H.R., 1981. Magmatic volatiles in explosive rhyolitic eruptions. Geophys. Res. Let., 8, 757-60.

Ewart, A., 1963. Petrology and petrogenesis of the quaternary pumice ash in the Taupo area, New Zealand. J. Petrol., 4, 392-431.

---------, 1966. Review of mineralogy and chemistry of the acidic volcanic rocks of the Taupo Volcanic Zone, New Zealand. Bull. Volcan., 29, 147-72.

Ewart, A., Green, D.C., Carmichael, I.S.E. and Brown, F.H., 1971. Voluminous low temperature rhyolitic magmas in New Zealand. Contrib. Mineral. Petrol., 33, 128-44.

Ewart, A., Hildreth, W. and Carmichael, I.S.E., 1975. Quaternary acid magma in New Zealand. Contrib. Mineral. Petrol., 51, 1-27.

Fisher, R.V., and Schmincke, H.U., 1984. Pyroclastic Rocks. Springer-Verlag, Berlin.

Froggatt, P.C., 1979. Lake Taupo- probable source of Taupo Pumice Formation (note). New Zealand J. Geol. Geophys., 6, 763-4.

--------, 1981. Stratigraphy and nature of Taupo Pumice Formation. New Zealand J. Geol. Geophys., 24, 231-48.

--------, 1982. Review of methods of estimating rhyolitic tephra volumes; applications to the Taupo Volcanic Zone, New Zealand. J. Volcan. Geother. Res., 14, 301-18.

Froggatt, P. ., Thesis

Gerlach, T.M., 1981. Restoration of new volcanic gas analyses from basalts of the Afar region: Further evidence of $CO_{2/@}$ degassing trends. J. Volcan. Geother. Res., 10, 83-91.

Haggerty, S.E., 1976. Opaque mineral oxides in igneous rocks. In D. Rumble III Ed., Oxide Minerals, p. Hg. 101-300. Mineral. Soc. Am. Short Course Notes.

Holloway, J.R., 1981. Volatile interactions in magma. In Newton, R.C., Navrotsky, A. and Wood, B.J., eds. Thermodynamics of minerals and melts. Springer-Verlag, Germany, 273-93.

Howorth, R., 1976. Late Pleistocene tephras of the Taupo and Bay of Plenty regions. Ph.D. thesis, Victoria Univ., Wellington, New Zealand.

Kilinc, I.A. and Burnham, .W., 1972. Partitioning of chloride between a silicate melt and coexisting aqueous phase from 2 to 8 kilobars. Econ. Geol., 67, 231-5.

Lindsley, D.H., and Spencer, K.J., 1982. Fe-Ti oxide geothermometry: Reducing analyses of co-existing Ti-magnetite (Mt) and Ilmenite (Ilm). Trans. Am. Geophys. Union, 63, 471.

Merzbacher, C. and Eggler, D.H., 1984. A magmatic geohydrometer: Applications to Mount St. Helens and other dacitic magmas. Geology, 12, 587-90.

Moore, J.C., 1970. Water content of basalt erupted on the ocean floor. Contrib. Mineral. Petrol., 28, 272-9.

Muenow, D.A., 1973. High temperature mass spectrometric gas-release studies of Hawaiian volcanic glass: Pele's Tears. Geochim. Cosmochim. Acta, 37, 1551-61.

Nairn, I.A., 1972. Rotoehu ash and the Rotoiti breccia formation, Taupo Volcanic zone, New Zealand. New Zealand J. Geol. Geophys., 15, 251-61.

----------, 1980. Source, age, and eruptive mechanism of Rotarua ash. New Zealand J. Geol. Geophys., 23, 193-207.

Nairn, I.A., 1981. Some studies of the geology, volcanic history, and geothermal resources of the Okataina volcanic center, Taupo volcanic zone, New Zealand. Ph.D. thesis, Victoria Univ., Wellington, New Zealand.

Peck, L. ., 1964. Systematic analysis of silicates. U.S. Geol. Surv. Bull., 1170, 89pp.

Rampino, M.R. and Self, S., 1984. Sulfur-rich volcanic eruptions and stratospheric aerosols. Nature, 310, 677-9.

Reid, F., 1983. Origin of the rhyolitic rocks of the Taupo Volcanic Zone, New Zealand. New Zealand J. Geol. Geophys., 15, 315-38.

Roedder, E., 1979. Origin and significance of magmatic inclusions. Bull. Mineral., 102, 487-510.

----------, 1984. Fluid Inclusions. Reviews in Mineralogy, ed. Paul H. Ribbe, volume 12.

Rutherford, N.F. and Heming, R.F., 1978. The volatile component of quaternary ignimbrite magmas from the North Island, New Zealand. Contrib. Mineral. Petrol., 65, 401-11.

Self, S., and Sparks, R.S.J., Characteristics of widespread pyroclastic deposits formed by the interaction of silicic magma and water, Bull. Volcan., 41, 196 212.

Sommer, M.A., 1977. Volatiles $H_{2/@O}$, $CO_{2/@}$ and CO in silicate melt inclusions in quartz phenocrysts from the rhyolitic Bandelier air-fall and ash-flow tuff, New Mexico. J. Geol., 85, 423-32.

Sommer, M.A. and Schramm, L.S., 1983. An analysis of the water concentrations in silicate melt inclusions in quartz phenocrysts from the Bandelier Tuff, Jemez Mountains, New Mexico. Bull. Volcan., 46, 299-320.

Stern, C.R. and Wyllie, P.J., 1978. Phase compositions through crystallization intervals in basalt-andesite-$H_{2/@O}$ at 30 kb. with implications for subduction zone magmas. Am. Mineral., 63, 641-62.

Stolper, E., 1982. Water in silicate glasses: an infrared spectroscopy study. Contrib. Mineral. Petrol., 81, ' 17.

Stormer, J.C., 1983. The effects of recalculation on estimates of temperature and oxygen fugacity from analyses of multicomponent iron-titanium oxides. Am. Mineral., 68, 586-94.

Taylor, B.E., Eichelberger, J.C., and Westrich, H.R., 1983. Hydrogen isotopic evidence of rhyolitic magma degassing during shallow intrusion and eruption. Nature, 306, 541-45.

Topping, W.W. and Kohn, B.P., 1973. Rhyolitic tephra marker beds in the Tongariro area, North Island, New Zealand. New Zealand J. Geol. Geophys., 16, 375-95.

Vucetich, C.G. and Howorth, R., 1976. Proposed definition of the Kawakawa tephra, the c. 20,000 years B.P. marker horizon in the New Zealand region. New Zealand J. Geol. Geophys., 19, 43-50.

Vucetich, C.G. and Pullar W.A., 1973. Holocene tephra formations erupted in the Taupo area, and interbedded tephras from other volcanic sources. New Zealand J. Geol. Geophys., 16, 745-80.

Walker, G.P.L., 1980. The Taupo Pumice: product of the most powerful known (ultraplinian) eruption? J. Volcan. Geother. Res., 8, 69-94.

----------, 1981. Characteristics of two phreatoplinian ashes, and their water-flushed origin. J. Volcan. Geother. Res., 9, 395-407.

Walker, G.P.L., Self, S. and Froggatt, P.C., 1981. The ground layer of the Taupo Ignimbrite: A striking example of sedimentation from a pyroclastic flow.

Wasserburg, G.J., 1957. The effect of H_2O in silicate systems. J. Geol., 65, 15-23.

Watson, E.B., 1976. Glass inclusions as samples of early magmatic liquid: determinative method and application to a South Atlantic basalt. J. Volcan. Geother. Res., 1, 73-84.

Wilson, C.N.J., Ambraseys, N.N., Bradley, J. and Walker, G.P.L, 1980.

A new date for the Taupo eruption, New Zealand. Nature, 288, 252-3.

Wilson, C.N.J., Rogan, A.M., Smith, I.E.M, Northey, D.J., Nairn, I.A., and Houghton, B.F., 1984. Caldera volcanoes of the Taupo Volcanic Zone, New Zealand. J. Geophys. Res., 89, 8463-84.